Coordination Chemistry Reviews 253 (2009) 1627–1648

Contents lists available at ScienceDirect

Coordination Chemistry Reviews

journal homepage: www.elsevier.com/locate/ccr

Review

Luminescence properties of phosphinegold(I) halides and thiolates

Edward R.T. Tiekink[a], Jun-Gill Kang[b,*]

[a] Department of Chemistry, The University of Texas at San Antonio, One UTSA Circle, San Antonio, TX 78249-0698, USA
[b] Department of Chemistry, Chungnam National University, 220 Gung-domg, Yusung-gu, Daejeon 305-764, Republic of Korea

Contents

ARTICLE INFO

Article history:
Received 5 November 2008
Accepted 16 January 2009
Available online 24 January 2009

Keywords:
Phosphinegold(I)
Luminescence
Structural motif

ABSTRACT

Mono- and multi-nuclear phosphinegold(I) compounds, incorporating halide and thiolate ligands, have attracted considerable interest owing to their unique luminescence properties. Assignments for the observed luminescence are summarized in terms of metal-centered transitions, intra-ligand transitions, and ligand-to-gold charge transfer transitions. Furthermore, Au. . .Au (i.e. aurophilic) interactions, sometimes observed in their solid-state structures, can also influence the observed luminescence characteristics. The aim of this review is to delineate the luminescent properties of the phosphinegold(I) halides and phosphinegold(I) thiolates, in particular where there is some debate as to the underlining optical processes responsible for this phenomenon and to relate these assignments to different structural motifs, in particular to the presence of aurophilic (Au. . .Au) interactions.

1. Introduction

One of the main motivating factors behind continuing studies of gold(I) compounds, often containing phosphine and thiolate or halide ligands, relates to their demonstrated and characteristic luminescence. Luminescence properties of these compounds are correlated with their unique photophysical and photochemical properties [1–7]. Accordingly, the luminescence properties of phosphinegold(I) compounds have been extensively investigated and a wide variety transitions, e.g. intra-ligand transitions, metal-centered transitions and ligand-to-metal charge transfer, are thought responsible for these properties. Additional interest in these systems arises as a result of the presence of aurophilic (i.e. Au. . .Au) interactions. Aurophilic interactions are known to be very important in the structural chemistry of gold, including phosphinegold(I) compounds [8,9]. Relativistic effects are responsible for aurophilic interactions [10,11] and it is well documented that these can provide a similar energy of stabilization to crystal packing as do hydrogen bonding interactions [12]. In terms of the overall theme of this review, aurophilic interactions, when present, are known to influence the luminescence properties exhibited in certain phosphinegold(I) compounds [13] as these enhance the transition probability and lower the energy gap between the emitting and receiving energy levels. In most phosphinegold(I) thiolates, the luminescence properties are determined mainly by the nature of the thiolate ligand. Although the phosphine ligand often contains a chromophore, the optical processes predominantly occur via the excitation of sulfur with subsequent charge transfer to gold. Another important tool utilized to understand the nature of the absorbing and emitting states are quantum mechanical calculations on the electronic structures and transitions. Herein, a full range of phosphinegold(I) halide and phosphinegold(I) thiolate compounds are discussed so as to provide an assessment of their luminescence properties. In latter sections, the assignments of luminescence are described for several series of phosphinegold(I) thiolates. In order to ascertain the influence of transitions due to the phosphinegold(I)

* Corresponding author. Tel.: +82 42 821 6548; fax: +82 42 821 8896.
E-mail address: jgkang@cnu.ac.kr (J.-G. Kang).

0010-8545/$ – see front matter © 2009 Elsevier B.V. All rights reserved.
doi:10.1016/j.ccr.2009.01.017

moieties upon luminescence in these compounds, the luminescence characteristics of phosphinegold(I) halides are reviewed first.

2. Phosphinegold(I) halides

Mononuclear triorganophosphinegold(I) halides provide relatively simple molecular structures for understanding how the gold(I) ion and the phosphine ligand are involved in optical processes, an important prelude before ascribing, with confidence, the source of the luminescence in the phosphinegold(I) thiolates described below. While the structural characteristics of the phosphinegold(I) halides are relatively homogeneous in terms of molecular geometry, their supramolecular aggregation via aurophilic (Au. . .Au) interactions is variable. While most structures adopt one of two motifs, a total of four supramolecular aggregation patterns are discerned in their crystal structures.

The structure of one of these prototype structures, Cy_3PAuCl, is illustrated in Fig. 1a; this is termed motif I for the R_3PAuX structures. Here, it is evident that the gold(I) center exists in a linear geometry defined by the phosphorus [Au–P 2.242(3) Å] and chloride [2.279(4) Å] atoms [14]; the angle subtended at the gold atom is 177.0(1)°. The second prototypical structure (motif II) is exhibited by Et_3PAuCl which features Au–P [2.232(11) and 2.231(9) Å; there are two independent molecules], Au–Cl [2.306(8) and 2.306(8) Å] distances, and linear P–Au–Cl angles [178.5(3)° and 178.9(3)°] but with the additional feature of an Au. . .Au interaction as highlighted in Fig. 1b [15]. The Au. . .Au distance of 3.568(2) Å is at the upper end of the generally excepted range of intermolecular Au. . .Au interactions, but is certainly indicative of supramolecular association between the molecules. The differences between motifs I and II are ascribed to the steric effects associated with the phosphine ligands [16].

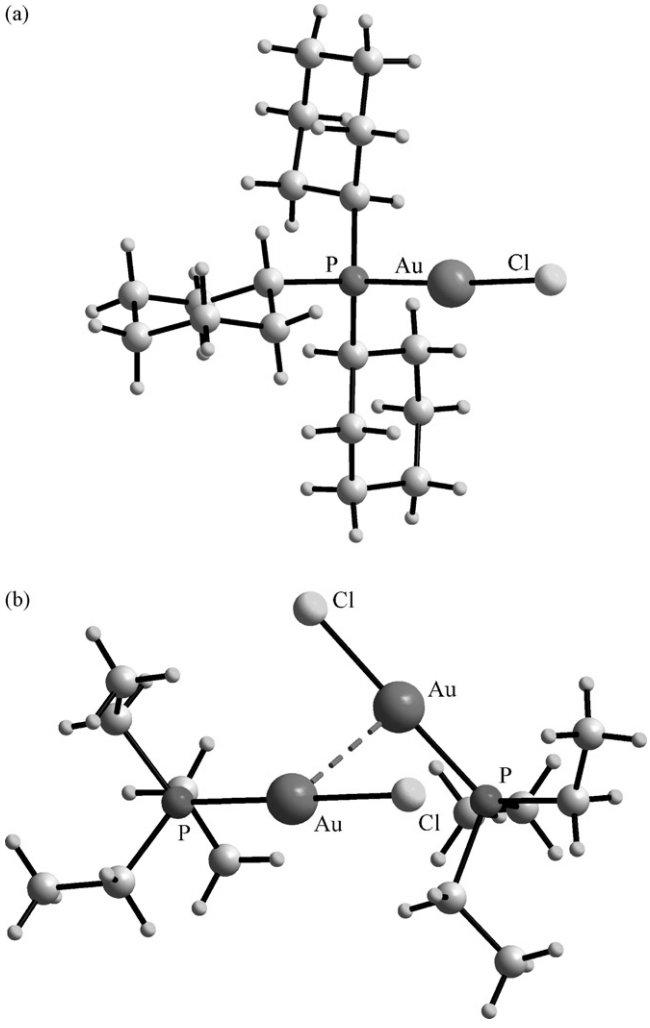

Fig. 1. (a) Molecular structure of Cy_3PAuCl [14], representing motif I for R_3PAuX structures, highlighting the linear coordination geometry for the gold atom; and (b) molecular structure of Et_3PAuCl [15], representing motif II, showing an intermolecular aurophilic (Au. . .Au) interaction as a dashed bond so that the molecule is formulated as $\{Et_3PAuCl\}_2$.

The isomorphous series of Ph_3AuX structures, for X = Cl [17], Br [18], and I [18a,19], adopt the motif I structure. In this series, there is little variation in the Au–P distances [2.233(1), 2.250(5) and 2.254(4) Å, respectively] and the expected monotonic increase in Au–X [2.278(1), 2.406(3) and 2.5555(16) Å] is observed; the P–Au–X angles lie in the narrow range 179.71(9) [X = Cl] to 178.4(1)° [X = I]. For the o-tolyl derivative $(o\text{-tolyl})_3PAuCl$, monoclinic (*C*2/*c*) and orthorhombic (*Pbca*; two independent molecules) polymorphs are known [20]. Despite the possibilities of variations in geometric parameters for $(o\text{-tolyl})_3PAuCl$, the Au–P, Au–Cl and P–Au–Cl parameters are experimentally equivalent [i.e. 2.235(4)–2.243(3) Å, 2.270(4)–2.289(4) Å, and 178.6(1)–179.4(1)°] and, experimentally equivalent to those in the structure of Ph_3PAuCl [17], see above. The following is an overview of the luminescence characteristics of these compounds.

The Ph_3PAuX (X = Cl and Br) compounds, where the bulky phosphine ligand prevents the formation of Au. . .Au interactions, when excited in UV region produce two emission bands in the 350–500 and 420–600 nm regions, respectively [21]. The excitation and emission data for Ph_3PAuX are listed in Table 1. The temperature dependence of the two emission bands is different. At room temperature, the high-energy band appeared as a trace. With decreasing temperature, the high-energy band gained in intensity and was strongly influenced by vibronic splitting at low temperature, while the low-energy band displays the opposite trends. The decay time of the high-energy emission is shorter than that of the low-energy emission, but is still longer than a sub-millisecond. The long lifetimes support the notion that the two emissions correspond to phosphorescence phenomena. By contrast, the excitation spectra of the two emission bands are quite similar. The excitation spectrum of the low-energy emission can be resolved into two components with peak positions at approximately 280 and 340 nm. These excitation bands were assigned as phenyl-localized $^1\pi\pi^*$ and $^3\pi\pi^*$ excited states, respectively. According to SCF–Xα–SW calculations for the ground-state orbitals of the model compounds H_3PAuCl, $H_2PhPAuCl$, Ph_3PAuCl and $PhPH_3^+$, the highest occupied molecular orbital (HOMO) comprises mainly phenyl-π character, while the lowest unoccupied molecular orbital (LUMO) is centered mainly on the gold, phosphorus and chloride atoms. Based on the HOMO–LUMO transitions, the high-energy emission was attributed to the ^{3}IL transition (IL = intra-ligand), while the low-energy emission remains to be assigned. The low-energy emission with a long lifetime and small zero-field splitting was not consistent with either a ^{3}LMCT or a ^{3}MLCT assignment involving a gold center.

Recently, the spectroscopic properties of $(o\text{-tolyl})_3PAuCl$ were also investigated, both experimentally and theoretically [22]. Representative spectra for $(o\text{-tolyl})_3P$ and $(o\text{-tolyl})_3PAuCl$ are shown in Fig. 2 and the excitation and emission data are summarized in Table 1. The absorption and the reflection spectra of $(o\text{-tolyl})_3PAuCl$ are quite different from those of the uncoordinated $(o\text{-tolyl})_3P$ molecule. For $(o\text{-tolyl})_3PAuCl$, there are three characteristic bands in the visible–UV region. The weak A-band, appearing in the 370–420 nm region, is not found for the $(o\text{-tolyl})_3P$ molecule. The B-band, 300–370 nm, has moderate intensity and the C-band, peaking at 280 nm, has high intensity. When excited in the UV region, both species produce luminescence in the region 350–700 nm. The main peak position is very close to that in $(o\text{-tolyl})_3P$ but much

Table 1
Emission and excitation data for selected phosphinegold(I) halides in the solid-state.

Compound	Au. . .Au (Å)	Excitation (nm)	Emission (nm)	Ref.
Ph_3PAuCl[a]		280(m), 330(s)	395(s), 485(sh)	[21]
Ph_3PAuBr[a]		280(w), 330(s)	390(s), 460(sh)[c]	[21]
$(o\text{-tolyl})_3P$[b]		300(sh), 340(s)	442(s), 570(sh)	[22]
$(o\text{-tolyl})_3PAuCl$[b]		306(s), 330(w), 380(m)	430(s), 490(w)	[22]
$[(Me_2PhP)AuCl]_2$[c]	3.2623(16)	313	360	[26]
$[(Me_2PhP)AuBr]_2$[c]	3.120(2)	313	360, 720	[26]
$[(Me_2PhP)AuI]_2$[c]	3.1063(17)	313	361, 645	[26]
$[(Me_2PhP)AuCl]_3$[c]	3.0916(19), 3.120(2)	313	361, 635	[26]

[a] $T = 1.4$ K.
[b] $T = 10$ K.
[c] RT.

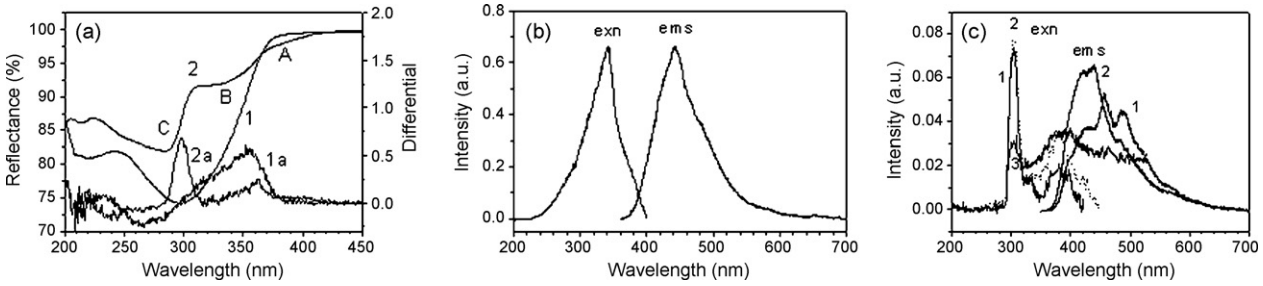

Fig. 2. (a) Reflectance and differential spectra of $(o\text{-tolyl})_3P$ (1, 1a) and $(o\text{-tolyl})_3PAuCl$ (2, 2a) at RT; (b) emission ($\lambda_{exn} = 348$ nm) and excitation ($\lambda_{ems} = 438$ nm) spectra of $(o\text{-tolyl})_3P$ at 78 K; and (c) emission ($\lambda_{exn} = 1$: 304 nm, 2: 343 nm) at $T = 78$ K and excitation ($\lambda_{ems} = 1$: 458 nm, 2: 490 nm, 3: 565 nm) of $(o\text{-tolyl})_3PAuCl$ at 78 K. Modified with permission from Ref. [22]. ©(2006) Korean Chemical Society.

weaker, and the spectroscopic shape is dependent on the excitation energy. The 343-nm excitation produces a main emission band, peaking at 430 nm, and a broad shoulder at the low-energy side, while the 304 nm excitation produces bell-type emission bands (426, 455, and 487 nm) with a low-energy shoulder and a spectroscopic range very close to that of the free $(o\text{-tolyl})_3P$ molecule. These observations were originally interpreted to indicate that the observed luminescence of $(o\text{-tolyl})_3PAuCl$ is due to an intra-ligand emission from $(o\text{-tolyl})_3P$. However, this hypothesis was ruled out after a comparison of the excitation spectra. As shown in Fig. 2b and c, the two spectra are very different. For $(o\text{-tolyl})_3PAuCl$, the excitation spectrum at 458 nm emission shows three bands, peaking at 305, 325, and 375 nm. In contrast, only one such excitation band was observed for $(o\text{-tolyl})_3P$. In $(o\text{-tolyl})_3PAuCl$, the 305 nm band is very strong and narrow, while the others are weak and broad. The species $(o\text{-tolyl})_3PAuCl$ does not exhibit the 280 nm excitation band which was occurs in each of Cy_3PAuCl and Ph_3PAuCl. The shape of this excitation spectrum is almost identical to that of the differential reflection spectrum shown in Fig. 2a. The strong 305 nm excitation corresponds to the C-absorption band and the weak bands, appearing in the 350–450 and 315–350 nm regions, were attributed to the A- and B-absorptions, respectively. The substitution of a methyl group at the ortho-position, compared with the triphenylphosphine analog, resulted in a red-shift in the peak positions of the A-band excitation and emission by approximately 4000 and 2100 cm^{-1}, respectively, as well as an increase in intensity of the C-band excitation.

Ab initio molecular orbital calculations [22] on the molecular orbitals and excited states of gas-phase $(o\text{-tolyl})_3PAuCl$ were performed to provide assignments for the observed spectroscopic properties. The molecular structure was fully optimized by a post-Hartree–Fock (HF) method for the ground state and CIS for the excited state; key results are summarized in Tables 2 and 3, respectively. The optimized geometry of the molecule conforms to C_3

Table 2
Partial molecular orbital compositions for $(o\text{-tolyl})_3PAuCl$.

MO	eV	Contribution (%) $(o\text{-toly})_3P$					Comment
		Au	P	18C	3C	Cl	
*l*7	0.24	0	0	100(p)	0	0	$C(p_x + p_y + p_z)$
*l*6	0.23	2(s) + 2(p)	5(s)	89(p)	0	0	$C(p_x + p_y + p_z)$
*l*5	0.23	3(p)	9(p)	7(s) + 78(p)	0	0	$C(p_x + p_y + p_z)$
*l*4	0.21	3(p)	9(p)	7(s) + 78(p)	0	0	$C(p_x + p_y + p_z)$
*l*3	0.16	50(s) + 8(d)	9(s) + 10(p)	0	0	5(s) + 3(p)	Au(s) + P(p)
*l*2	0.12	82(p)	0	2(s) + 2(p_z)	5(s) + 2(p)	6(p)	Au($p_y + p_z$)
*l*1	0.12	78(p)	0	3(s)	5(s) + 4(p)	6(p)	Au($p_y + p_z$)
*h*1	−0.29	2(s)	1(s) + 13(p)	79(p)	0	0	P(p_x) + C($p_y + p_y + p_z$)
*h*2	−0.31	0	0	93(p)	0	0	$C(p_x + p_y + p_z)$
*h*3	−0.31	0	0	93(p)	0	0	$C(p_x + p_y + p_z)$
*h*4	−0.31	0	0	93(p)	0	0	$C(p_x + p_y + p_z)$
*h*5	−0.32	0	0	89(p)	0	8(p)	$C(p_x + p_y + p_z)$
*h*6	−0.32	0	0	90(p)	0	8(p)	$C(p_x + p_y + p_z)$
*h*7	−0.32	1(p_z) + 7(d)	0	7(p)	0	86(p)	Cl($p_y + p_z$)
*h*8	−0.32	1(p_y) + 7(d)	0	7(p)	0	86(p)	Cl($p_y + p_z$)
*h*9	−0.34	19(s) + 12(d)	0	0	0	2(s) + 63(p_x)	Au(s + d_0 + $d_{\pm 2}$) + Cl(p_x)

symmetry (along *x*-axis), consistent with the earlier observations that non-symmetric experimental (crystallographic) structures optimize to symmetric calculated molecules in the absence of crystal packing effects [23]. The first six HOMO's, *h*1–*h*6, have π-orbital character of the o-tolyl groups with contributions greater than 80%. The next pair of doubly degenerate HOMO's, *h*7 and *h*8, effectively corresponds to the p_y and p_z orbitals of the chloride atom, each occupied by a lone-pair of electrons. The LUMO is the doubly degenerate *l*1 and *l*2, which arises from the linear combination of the p_y and p_z orbitals of gold. The next LUMO, *l*3, is the σ*-type orbital formed between the s and d_{xy} orbitals of the gold atom as well as the s and p_x orbitals of the chloride and phosphorus atoms. The contribution of the s orbital of the gold atom is as much as 50%. In Table 3, some excited states are classified in terms of A-, B-, and C-bands, according to the energy gap and the oscillator strength. In the group A, the first two excited states, 1E and 1A, arise from the electronic transitions from the chloride atom to gold. The transition probabilities from the ground state, X, to these two states are very small, giving rise to the first weak A-absorption. According to the atomic charges determined from a Mulliken population analysis, for the X → 1E transition, the atomic charges of gold and chloride change from 0.20 to −0.11 and from −0.53 to −0.11, respectively, while the change of the atomic charge of phosphorus is almost negligible. For the X → 1A transition, the changes of the electron atomic charges of gold and chloride are 0.23 and −0.27, respectively. These changes quite clearly indicate that these transitions are associated with charge transfer from chloride to gold. In group B, the transitions from the ground state to the 2E, 5A and 6A states comprise the B-absorption band. These transitions are associated with the electronic transitions from the π-system of the aromatic rings to the s, p_y and p_z orbitals of gold. Accordingly, the B-absorption band is attributed to charge transfer from the phenyl groups to the gold atom. As indicated in Table 3, the X → 4E and 5E transitions have large probabilities with $f = 0.396$ and $f = 0.122$, respectively. The 4E and 5E excited states predominantly arise from transitions from *h*9 to *l*1 and *l*2 and are attributed to the strong C-absorption band. This transition is primarily associated with the charge transfer from chloride to gold and to a lesser extent to the s → p transition in the gold atom. The charge densities of gold and chloride vary by 0.23 and −0.17, respectively, for X → 4E, indicating that the C-absorption band is mainly associated with the charge transfer from chloride to gold. Thus, the observed luminescence of $(o\text{-tolyl})_3PAuCl$ is strongly associated with the charge transfer from chloride to gold. As seen in the excitation spectrum, the strong C-band excitation ($\lambda_{exn} = 306$ nm) produces intense luminescence with the main components in the 375–550 nm region, while the weak A-band excitation ($\lambda_{exn} = 380$ nm) produce the weak luminescence in the low-energy side. Although the B-absorption band is more intense than that the A-absorption band, the B-band

Table 3
High-value CIS excited states and predominant transitions for $(o\text{-tolyl})_3PAuCl$.

Excited state	eV	*f*	Predominant transition
(A-band)			
1E	6.51	0.007	*h*7 → *l*3; *h*8 → *l*3
1A	7.00	0.008	*h*9 → *l*3
(B-band)			
2A, 3A	7.38	0.003	*h*7, *h*8 → *l*1, *l*2
4A	7.40	0	*h*7 → *l*2
2E	7.47	0.072	*h*1 → *l*1, *l*2
5A	7.48	0.065	*h*1 → *l*3; *h*3 → *l*5; *h*2 → *l*4
3E	7.56	0.009	*h*1 → *l*4, *l*5
6A	7.59	0.152	*h*1 → *l*3, *l*7; *h*2, *h*3 → *l*4, *l*5
(C-band)			
4E	7.88	0.396	*h*9 → *l*1, *l*2
5E	8.05	0.122	*h*9 → *l*1, *l*2; *h*1, *h*6 → *l*1, *l*2, *l*4, *l*5

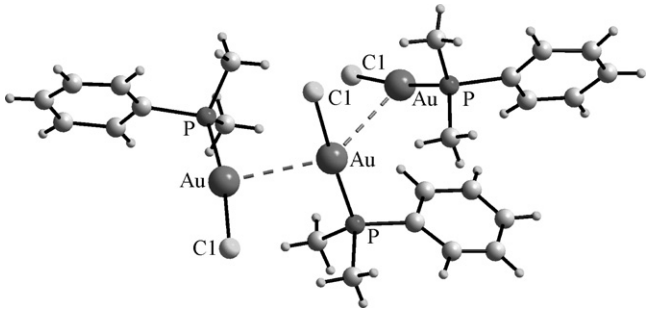

Fig. 3. Molecular structure of trimeric $(Me_2PhP)AuCl$ [26], or $\{(Me_2PhP)AuCl\}_3$, representing motif III for R_3PAuX structures; aurophilic interactions are represented by dashed lines.

excitation ($\lambda_{exn} = 330$ nm) produces a trace of luminescence. This indicates that the charge transfer from the π-system of phenyl groups to gold may be ineffective in producing an emission from $(o\text{-tolyl})_3PAuCl$. From the foregoing, it is clear that the characteristic optical-properties of the $(o\text{-tolyl})_3PAuCl$ compound are attributed to chloride to gold charge transfer for the absorption and vice versa for the emission. The following summarizes the influence of aurophilic interactions upon the optical process of phosphine-gold(I) halides, i.e. in cases where the steric bulk of the phosphine ligand is insufficient to preclude the formation of Au. . .Au interactions.

Using pseudo-potential methods, Pyykkö and co-workers predicted that the aurophilic attraction in $\{Ph_3PAuX\}_2$ increases in the series F < Cl < Br < I and they found that the calculated strength of the aurophilic interaction was strongly dependent on the type of basis set used in the quantum mechanical calculation [24]. The magnitude of the Au. . .Au interaction was strongly correlated with the Au. . .Au distance; the calculated Au. . .Au distances within two perpendicular units (i.e. with C_2 symmetry) were 3.41 Å for X = F, 3.37 Å for X = Cl, 3.34 Å for X = Br, and 3.32 Å for X = I. These trends were experimentally verified in the structures of molecules with the general formula $(Me_2PhP)AuX$. The $(Me_2PhP)AuX$ series of structures for X = Cl [25,26], Br and I [26] present aurophilic interactions in their crystal structures and a new structural motif. Similar trends in geometric parameters as for the Ph_3PAuX series described above are found so that Au–P in the X = Cl derivative [2.214(6) and 2.204(5) Å for two crystallographically independent molecules] is systematically shorter than in the X = Br [2.246(9) and 2.247(9) Å] and X = I [2.244(5) and 2.260(6) Å] species; the X = Br and I structures are isomorphous and each feature two independent molecules. The variations in the Au–X and P–Au–X parameters, again, are as expected. In each structure an aurophilic interaction occurs between the two independent molecules giving Au. . .Au separations that correlates with the decreasing electronegativity of the halide, i.e. 3.2623(16), 3.1193(21), and 3.1063(17) Å, respectively. Motif III for the R_3PAuX structures is found in a polymorph of $(Me_2PhP)AuCl$ [26]. As illustrated in Fig. 3, the trinuclear structure features two aurophilic interactions [3.0916(19) and 3.1202(2) Å] and so the compound might conveniently be formulated as $\{(Me_2PhP)AuCl\}_3$ as opposed to the dimeric species, $\{(Me_2PhP)AuX\}_2$, motif II; some non-systematic variations in the Au–P and Au–Cl distances in the structure of $\{(Me_2PhP)AuCl\}_3$ suggest the possibility of some contamination by bromide [26].

When excited in the UV region, the $\{(Me_2PhP)AuCl\}_n$ compounds produce two emission bands [26,27]. At reduced temperatures, the high-energy emission, appearing in the region 360–500 nm, gains significant intensity. The high-energy emission was attributed to the intra-ligand $^3\pi\pi^*$ phosphorescence of the phenyl moiety, as the case of mononuclear Ph_3PAuCl. This assignment is controversial, since $\{Et_3PAuCl\}_2$ also produced a

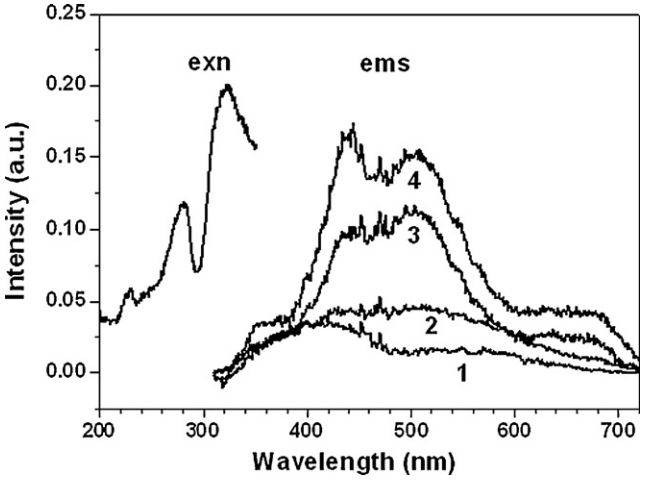

Fig. 4. Emission (λ_{exn} = 280 nm, T = 1: RT, 2: 150 K, 3: 70 K, 4: 10 K) and excitation (λ_{ems} = 455 nm, T = 10 K) spectra for Et_3PAuCl.

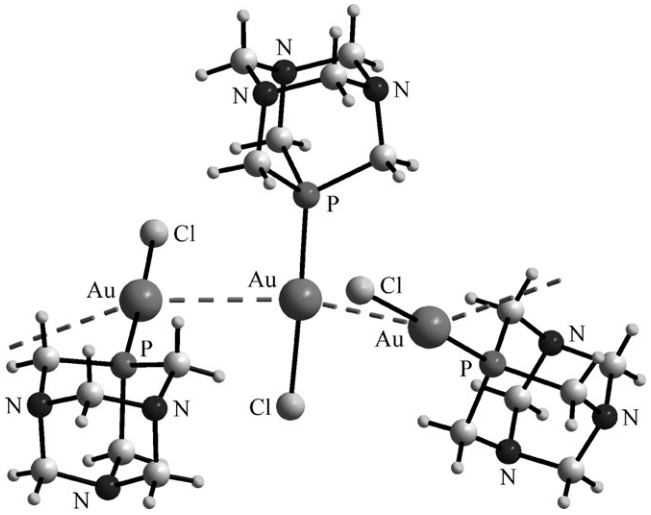

Fig. 5. Molecular structure of polymeric (PTA)AuCl [29], or $\{(PTA)AuCl\}_n$, representing motif IV for R_3PAuX structures; aurophilic interactions are represented by dashed lines.

high-energy emission, see Fig. 4. The low-energy band appeared in the region 550–700 nm for the dimeric bromide and iodide derivatives as well as for each of the dimeric and trimeric chloride compounds. Based on the results of SCF–Xα–SW calculations on the model compounds H_3PAuX and $\{H_3PAuX\}_2$, the low-energy bands were assigned to the LUMO–HOMO excitation. For the monomeric species, the excitation is mainly centered on the gold atom for the X = Cl compound, while it becomes a halide to gold charge transfer in X = Br and I. For the dimeric species, the gold-character in the HOMO decreases from 78% to 36% and the p-character of X increases from 10% to 58% in going from X = Cl to I. Accordingly, the observed low-energy band was assigned primarily due to the phosphorescence resulting from the gold-based $\sigma(p) \leftarrow \sigma^*(s, d)$ excitation with a smaller contribution from X → Au charge transfer. However, the SCF–Xα–SW method provides only limited information on the nature of the molecular orbitals, since it works best on spherical molecules. Therefore, the relative energies of the empty orbitals are unreliable [28]. The emission spectrum of the dimeric $\{Et_3PAuCl\}_2$ compound measured at various temperatures is illustrated in Fig. 4. At room temperature, when excited at 280 nm the compound produces a weak emission: a broad band in the 300–500 and a broad shoulder in the 500–700 nm. With decreasing temperature, the emission intensity increases and the spectroscopic shape is better resolved. The emission spectrum of $\{Et_3PAuCl\}_2$ comprises four components, peaking at 360, 440, 505, and 650 nm. The excitation spectra of these emissions are very similar and they can be resolved into three components, peaking at 230, 280 and 325 nm. The complexity in the emission might be due to the weak Au. . .Au interaction of 3.568(2) Å [15]. Quantum mechanical calculations on the structural and optical properties of Et_3PAuCl and $\{Et_3PAuCl\}_2$ are needed to provide accurate assignments for the observed complex pattern of luminescence observed for $\{Et_3PAuCl\}_2$.

The final structures to be described in this section contain the functionalized phosphine ligand 1,3,5-triaza-7-phosphaadamantane (TPA) [29,30]. The structure of (TPA)AuCl represents a fourth structural motif for R_3PAuX. As illustrated in Fig. 5, molecules aggregate into a supramolecular helical chain via Au. . .Au interactions [3.3960(6) Å]. The 1:1 acetonitrile solvate [30] reverts to the dimeric motif II. From acidic media, the protonated PTA species, formulated as $[(TPAH)AuCl]Cl{\cdot}0.5(H_2O)$ can be isolated [30], which adopts motif II. The latter two compounds present interesting luminescence characteristics that highlight the importance of aurophilic interactions [30]. Thus, upon excitation at 290 nm [(TPA)AuCl]·acetonitrile and $[(TPAH)AuCl]Cl{\cdot}0.5(H_2O)$ produce only the low-energy emissions, peaking at 674 and 596 nm, respectively. The large difference in the peak positions between two compounds was correlated with the magnitude of the Au. . .Au interaction, i.e. 3.0923(5) Å in [(TPA)AuCl]·acetonitrile and significantly longer at 3.320(2) Å in $[(TPAH)AuCl]Cl{\cdot}0.5(H_2O)$. Extended Hückel calculations on the MM2-minimized structures using the CAChe program indicated that the HOMO (σ_u orbital), comprising d_{z2} and s of gold, and p_z of phosphorus, became destabilized by dimerization of two monomeric units. Further, the shorter the Au. . .Au distance, the more destabilized became

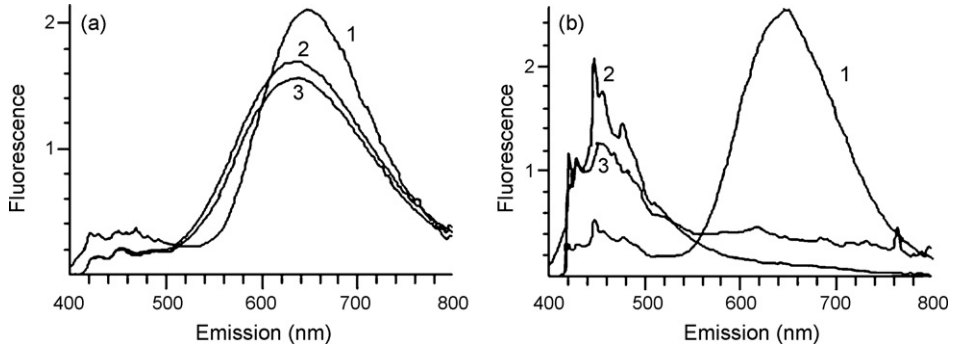

Fig. 6. (a) Temperature-dependent emission spectra of the low-energy band of (TPA)AuBr at (1) 78, (2) 200, and (3) 298 K excited at 320 nm; and (b) dependence of the emission spectra of (TPA)AuBr excitation wavelength: (1) excited at 320 nm at 78 K; (2) excited at 340 nm at 78 K; (3) excited at 340 nm at 298 K. Reproduced with permission from [31]. ©(1995) American Chemical Society.

the HOMO. As a consequence, the HOMO–LUMO gap decreases to result in the red-shift of the luminescence. The low-energy emission was attributed to the metal-centered phosphorescence [30].

For each of (TPA)AuX, for X = Br and I, the high-energy band also appeared with vibronic distortions in the 400–520 nm region [31]. The intensities of the two bands were very dependent on the excitation wavelength. A typical dependence of the intensity and the excitation spectra of the two emission bands are shown in Fig. 6. The emitting center of the high-energy band is different from that of the low-energy band. The vibronic spacing of 350–500 cm^{-1} is very close to the Au–X vibration appearing around 200–330 cm^{-1} rather than the Au–P stretching mode (380 cm^{-1}). This similarity led to the assignment of the high-energy emission band to a band originating from the halide to gold charge transfer excitation.

3. Binuclear and polynuclear phosphinegold(I) compounds

Polydentate phosphine ligands have the potential to bring into close proximity two or more gold atoms and therefore to encourage/stabilize the formation of aurophilic interactions. Thus, Au. . .Au separations are often in the range 2.80–3.10 Å depending on the geometry and electronic structure of the ligands [28,34–37]. The

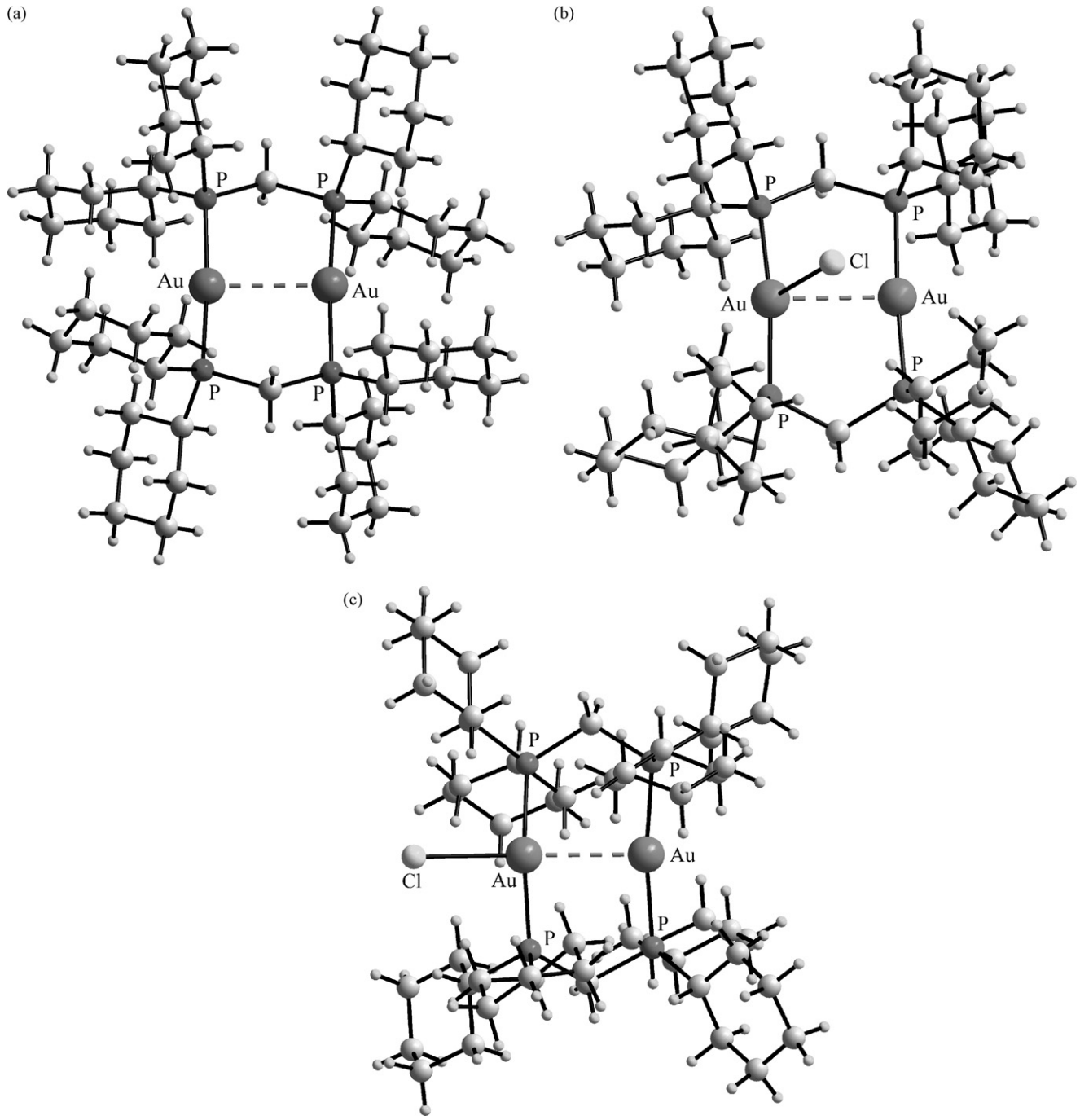

Fig. 7. (a) Molecular structure of the dinuclear dication in $\{Au_2[Cy_2PCH_2PCy_2]_2\}(ClO_4)_2$ [32], representing the common motif for structures containing $\{Au_2[Cy_2PCH_2PCy_2]_2\}^{2+}$, highlighting the linear coordination geometry for the gold atom, the formation of the eight-membered $[Au–P–C–P]_2$ ring, and the intra-molecular aurophilic (Au. . .Au) interaction as a dashed bond; (b) molecular structure of the first isomer for $\{Au_2[Cy_2PCH_2PCy_2]_2Cl\}Cl$ [33], with the chloride perpendicular to the Au. . .Au axis; and (c) molecular structure of the second isomer for $\{Au_2[Cy_2PCH_2PCy_2]_2Cl\}Cl$, with the chloride coincident with the Au. . .Au axis.

Table 4
Luminescence properties and Au. . .Au distances for selected binuclear phosphinegold(I) compounds at room temperature[a].

Compound	Au. . .Au (Å)	λ_{ems} (nm) in CH_3CN solution	λ_{ems} (nm), in the solid-state	Ref.
$[Au_2(\mu\text{-dcpm})_2](ClO_4)_2$	2.9138(9)–2.9389(8)	370(w), 510(s)	368(s), 564(w)	[32]
$[Au_2(\mu\text{-dcpm})_2](PF_6)_2$		370(w), 490(s)	368(s), 505(w)	[32]
$[Au_2(\mu\text{-dcpm})_2](SO_3CF_3)_2$		370(w), 490(s)	363(s)	[32]
$[Au_2(\mu\text{-dcpm})_2][Au(CN)_2]_2$	2.9877(6)	370(w), 495(s)	368(s), 515(w)	[32]
$[Au_2(\mu\text{-dcpm})_2]Cl_2$		370(w), 495(s)	513	[32]
$[Au_2(\mu\text{-dcpm})_2]I_2$	2.9509(10)–3.0755(12)	530	467	[32]
$[Au_2(\mu\text{-dppm})_2](BF_4)_2$	2.9309(16)	593	-	[28]
$[Au_2(\mu\text{-dppm})_2](BH_3CN)_2$	2.982(2)	–	571	[28]
$[Au_2(\mu\text{-dppm})_2]Cl_2$	2.9941(8)	–	467	
			500[b]	
			510, 680	[36]
–	–		530, 620(sh)[b]	
$[Au_2(\mu\text{-dppm})_2]I_2$			670	[36]
$[Au_2(\mu\text{-dpm})_2]^{2+}$[c]	3.17[d]/2.75[e]			[37]
$[Au_2(\mu\text{-dpm})_2(MeCN)_2]^{2+}$[c]	3.16[d]/2.72[e]		331, 557	[37]

[a] dcpm = bis(dicyclohexylphosphino)methane; dppm = bis(diphenylphosphino)methane; and dpm = bis(diphosphino)methane.
[b] T = 12 K.
[c] Calculated structures.
[d] Au. . .Au for the ^1A_g ground-state.
[e] Au. . .Au for the ^3A_u excited-state.

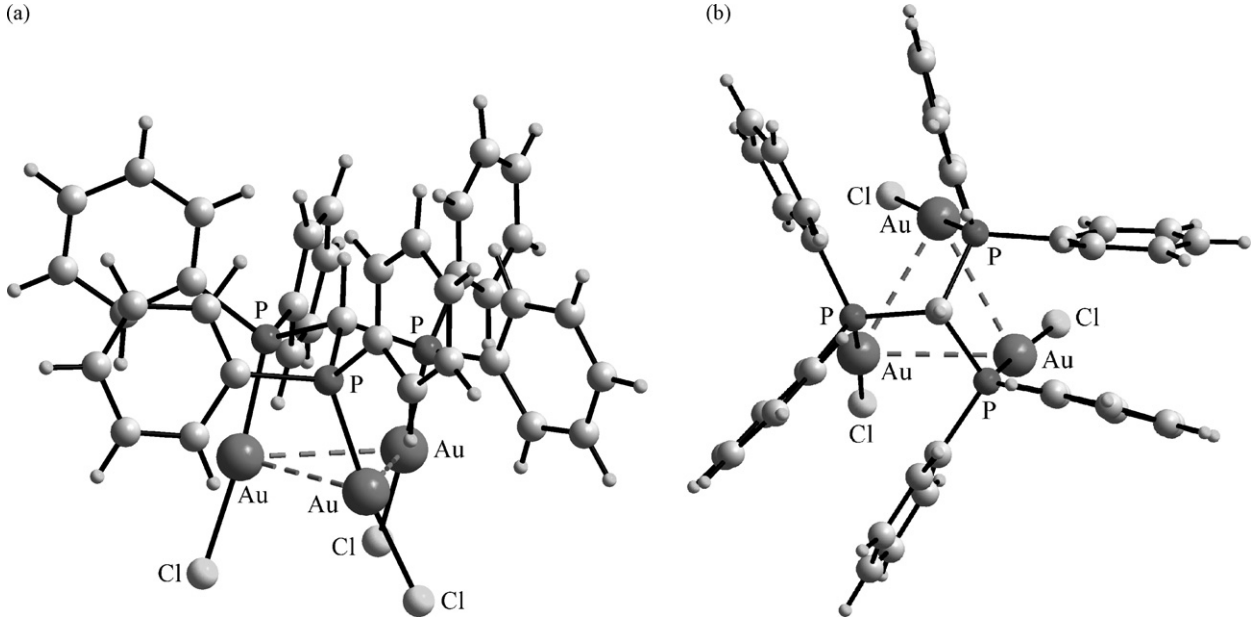

Fig. 8. (a) Side-on and (b) plan view of the molecular structure of trinuclear $HC[PPh_2(AuCl)]_3$ [38]; aurophilic interactions are represented by dashed lines.

bidentate ligands bis(dicyclohexylphosphino)methane (dcpm) and bis(diphenylphosphino)methane (dppm) provide good examples of this principle and at the same time display fascinating structural features. In the series of structures $[Au_2(\mu\text{-dcpm})_2]^{2+}$, for counter ions ClO_4^-, $[Au(CN)_2]^-$ and I^- [32], a centrosymmetric eight-membered $[Au–P–C–P]_2$ ring is formed each with a flattened chair conformation as the methylene bridges lie above and below the Au_2P_4 plane (Fig. 7a). The Au–P distances lie in the relatively narrow range 2.3011(16)–2.343(3) Å. The respective counter-ions are at least 3.0 Å from the gold centers in these structures and no

Table 5
Luminescence properties and Au. . .Au distances for selected trinuclear phosphinegold(I) compounds at various temperatures[a].

Compound	Au. . .Au (Å)	λ_{ems} (nm)/τ (μs) in CH_2Cl_2 solution	λ_{ems} (nm) in the solid-state	Ref.
$HC[PPh_2(AuCl)]_3$	3.2104(7) (×3)	550/1.1	20 K: 500 298 K: 510, 680	[36,38]
$HC[PPh_2(AuI)]_3$	3.1355(18) (×3)	590/1.2	12 K: 480, 680 298 K: 680	[36]
$[Au_3(\mu\text{-dpmp})_2Cl_2]Cl$	2.947(3), 2.963(3)	650/1.2	77 K: 485, 620	[36]
$[Au_3(\mu\text{-dpmp})_2I_2]I$	2.9525(9), 3.0202(9)	660/2.5	12 K: 575, 665	[36]
$[Au_3(\mu\text{-dpmp})_2Cl](PF_6)_2$	2.9293(18), 2.9592(16)	469(s)	–	[39]
$[Au_3(\mu\text{-dpmp})_2Br](PF_6)_2$	2.9341(18), 2.9650(17)	518(vw)	–	[39]
$[Au_3(\mu\text{-dpmp})_2I](PF_6)_2$	2.9273(16), 2.9415(16)	460(sh), 551(s)	–	[39]

[a] dpmp = bis(diphenylphosphinomethyl)phenylphosphine.

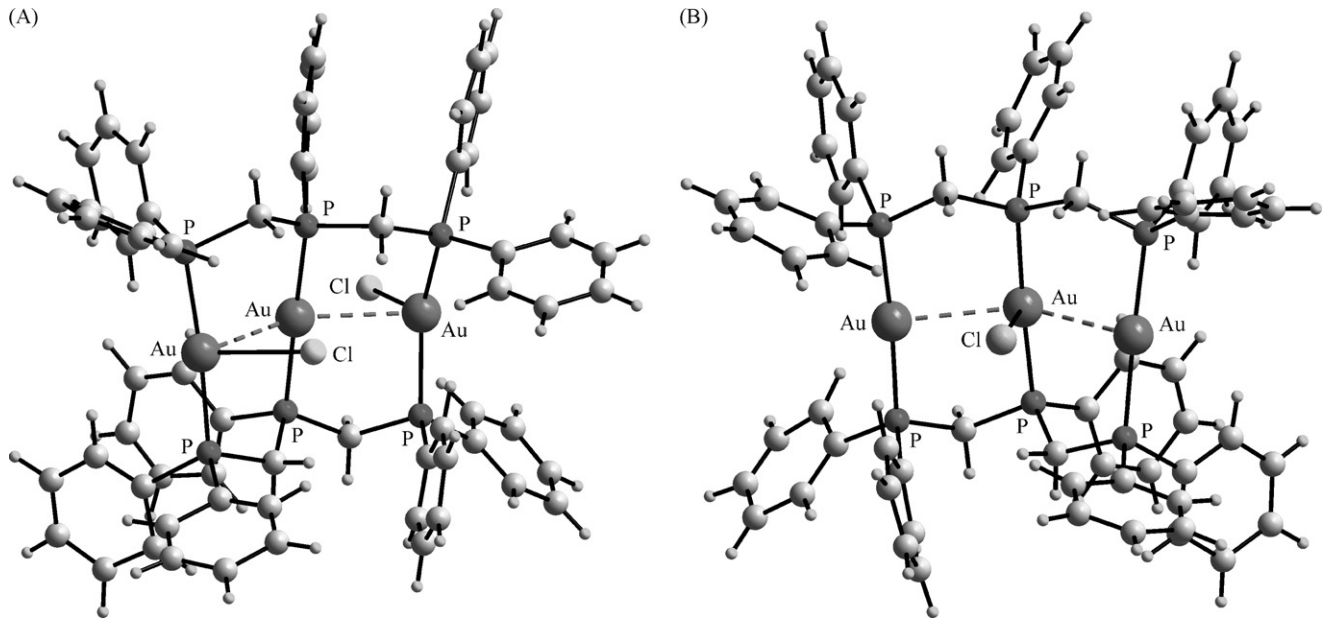

Fig. 9. Molecular structures of (a) the trinuclear cation in $[Au_3(\mu\text{-dpmp})_2Cl_2]Cl$ [36]; and (b) the trinuclear dication in $[Au_3(\mu\text{-dpmp})_2Cl](PF_6)_2$ [39]; aurophilic interactions are represented by dashed lines.

apparent correlation exists between the magnitude of the Au...X separation and the Au–P distance so that to a first approximation the dications for this series can be described as "isolated". The Au...Au separations vary from a short 2.9138(9) to 3.0755(12) Å. A structural variation occurs for the Cl^- [33] derivative (methanol solvate) in that one of the chloride counter ions is formally associated with a gold atom.

The $\{Au_2[Cy_2PCH_2PCy_2]_2Cl\}Cl$ compound [33] presents an interesting situation in that within the one crystal, two distinct isomers co-crystallize. In one isomer, the chloride atom is perpendicular to the Au...Au axis, (Fig. 7b), and in other, the chloride ion lies on this axis, (Fig. 7c). Three pairs of Au–P distances lie in the narrow range 2.3056(8)–2.3093(9) Å with the exceptional pair being longer at 2.3261(9) and 2.3274(8) Å, and involve the gold atom connected to the chloride atom coincident with the Au...Au axis. A direct consequence of this elongation is seen in the lengthening of the Au...Au separation in this isomer, i.e. 2.9923(2) Å, compared with 2.9444(2) Å. Reducing the steric bulk of the dcpm ligand by replacing the cyclohexyl rings with phenyl rings to yield bis(diphenylphosphino)methane (dppm) does not result in any significant structural differences, Table 4.

In terms of luminescence characteristics, the magnitude of the Au...Au interaction is presumed to exert a significant effect upon the low-energy emission as for the monomeric phosphinegold(I) halides described in Section 2. As collated in Table 4, the prototype compounds, i.e. $[Au_2(\mu\text{-dcpm})_2]^{2+}$ and $[Au_2(\mu\text{-dppm})_2]^{2+}$, exhibit luminescence properties that are very significantly affected by counter anions, taking into account that the Au...Au separations are almost constant. For $[Au_2(\mu\text{-dcpm})_2]^{2+}$, the 280 nm excitation produces an intense high-energy emission or/and a low-energy emission, depending on the counter anion with the high- and low-energy emission maxima appearing in the 363–368 and 467–564 nm regions, respectively. For halide counter anions, only the low-energy emission appeared at 513 nm for X = Cl and 467 for X = I [32]. The lifetimes for both high- and low-energy emissions are in the range of 1.0–7.0 μs at room temperature. Using $[Au_2(\mu\text{-dpm})_2]^{2+}$ and $[Au_2(\mu\text{-dpm})_2{}^+(MeCN)_2]^{2+}$ (dpm = bis(diphosphino)methane) as model compounds, i.e. dinuclear compounds without and with solvated acetonitrile, respectively, Zhang and Che [37] performed *ab initio* molecular orbital calculations to determine the electronic structure and spectroscopic properties. The ground- and excited-state structures were optimized by second-order Møller–Plesset (MP2) and the CIS methods, respectively. The results, summarized in Table 4, revealed that the aurophilic interaction was very weak in the ^1A_g ground-state and became significantly stronger in the ^3A_u excited-state. This excited-state was attributed to the emitting level of the observed low-energy emission. The energy level of this emitting-state was varied by the interaction between the gold atom and solvent molecule and/or neighboring anion in the excited state. The CIS calculations showed that in the absence of

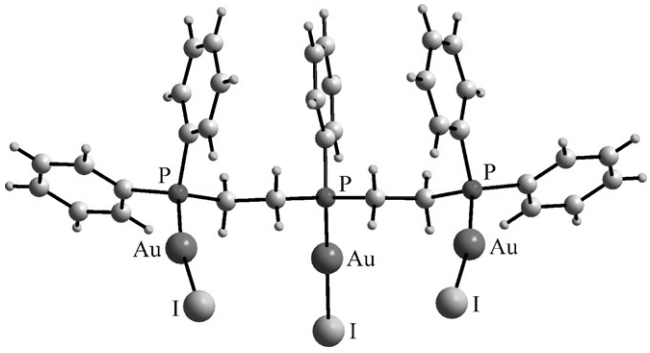

Fig. 10. Molecular structure of the trinuclear $[(\mu\text{-triphos})(AuI)_3]$ [40].

Table 6
Emission and excitation maxima (nm) of triphos and selected $[(\mu\text{-triphos})(AuX)_3]$ compounds measured at 278 and 77 K [41][a].

Compound	278 K		77 K	
	Excitation	Emission	Excitation	Emission
Triphos	240–290	425	240–290	425
$[(\mu\text{-Triphos})(AuCl)_3]$			330	440
$[(\mu\text{-Triphos})(AuBr)_3]$	350	475	335	455
$[(\mu\text{-Triphos})(AuI)_3]$	385	525	340	460
$[(\mu\text{-Triphos})(AuC_6F_5)_3]$			325	450
			255	430

[a] Triphos = bis(diphenylphosphinoethyl)phenylphosphine.

the aurophilic interaction the $^3A_u((sp)_\sigma) \rightarrow {}^1A_g(d_{\sigma^*})$ transition was responsible for the high-energy emission. For very bulky phosphine ligands, the counter anion is too distant from the gold centers to vary the wavelength of the high-energy emission. In addition, CIS calculations on the transitions from the X^1A_g ground state to the three low-lying ^1A_u excited states revealed that for the $X^1A_g \rightarrow A$ and C^1A_u transitions, only the population of the gold atom changes. In the $X^1A_g \rightarrow B^1A_u$ transition, a change in the population of the cyanide group of the acetonitrile molecule was indicated. Based on the results of the CIS calculations, the A- and C-absorption bands were attributed to the $d_{\sigma^*} \rightarrow p_\sigma$ and $d_{\sigma^*} \rightarrow (sp)_\sigma$ transitions, respectively. As indicated in Table 4, in solution the compounds also exhibit low- and/or high-energy emission bands.

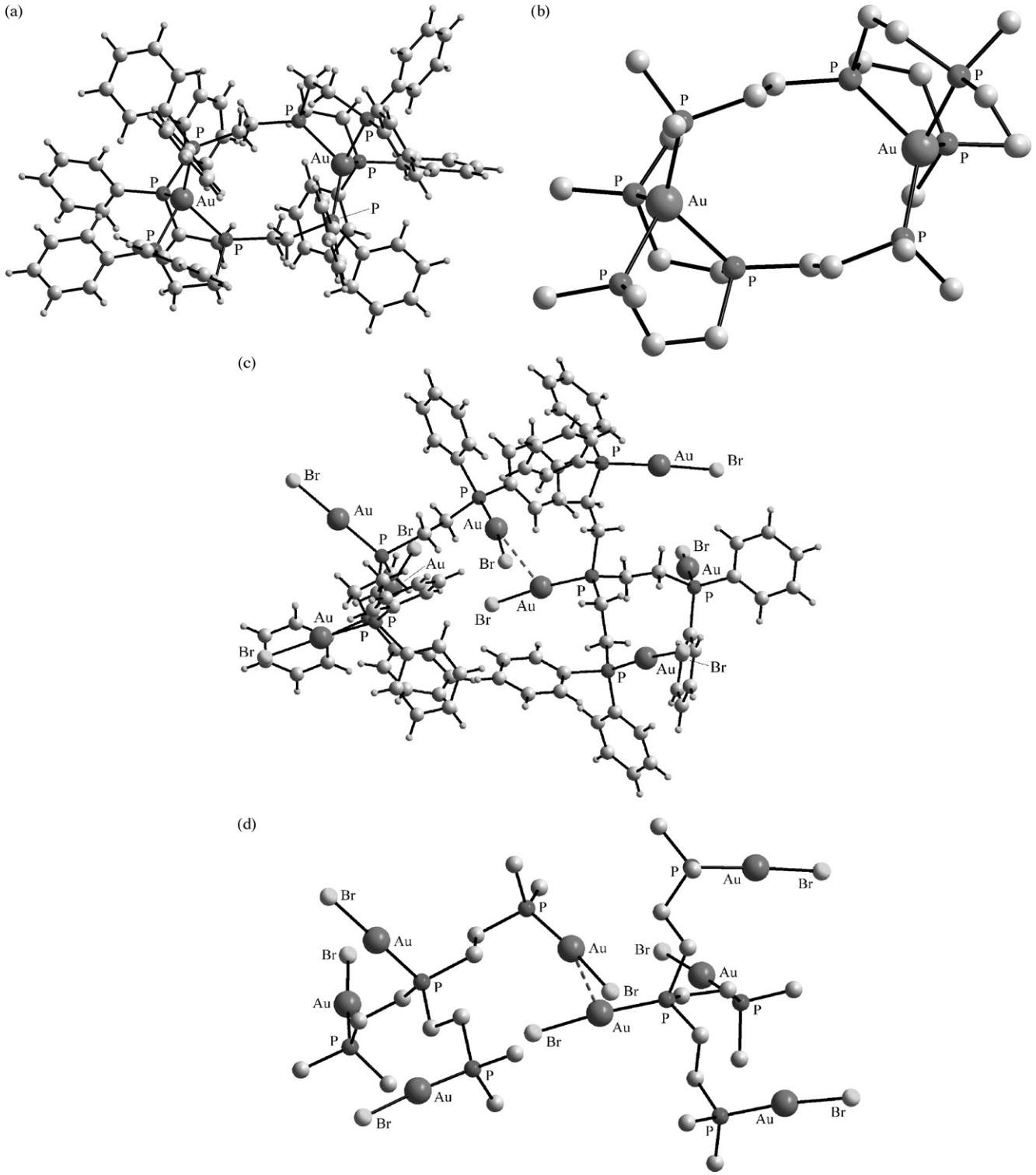

Fig. 11. Molecular structures of (a) the dinuclear dication in $[Au_2(\mu\text{-dpep})_2]Cl_2{\cdot}2CHCl_3$ [42]; (b) a simplified view of $[(\mu\text{-dpep})_2Au_2]^{2+}$ [42] showing only ipso-carbon atoms of the phenyl rings and with all hydrogen atoms omitted for clarity; (c) the tetranuclear structure of $[(\mu\text{-dpep})(AuBr)_4]$; and (d) a simplified view of $[(\mu\text{-dpep})(AuBr)_4]$ [42] showing only ipso-carbon atoms of the phenyl rings and with all hydrogen atoms omitted for clarity; aurophilic interactions are represented by dashed lines.

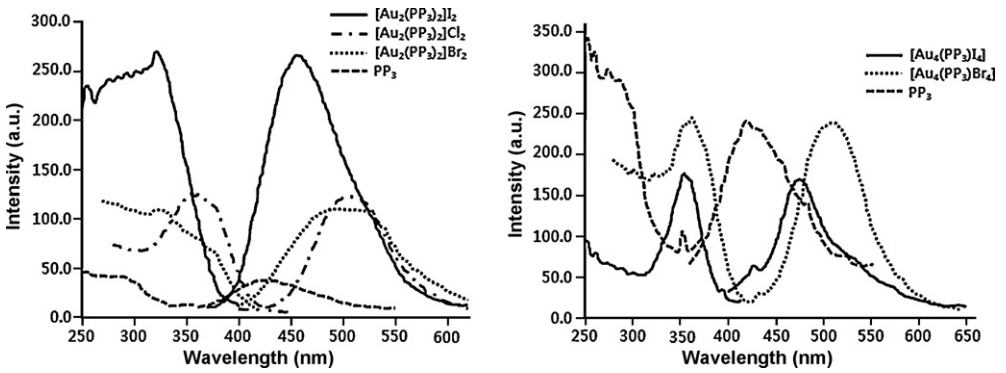

Fig. 12. (a) 77 K solid-state excitation and emission spectra of dpep (-.-.-) and $[Au_2(\mu\text{-dpep})_2]X_2$ [X = Cl (—), Br (· ·) and I (––), using a 1% intensity attenuator; and (b) solid-state excitation and emission spectra of the dpep (-.-.-)) and $(\mu\text{-dpep})(AuX)_4$ [X = Br (—) and I (––))] at 77 K. Reproduced with permission from [43]. ©(2008) Royal Society of Chemistry.

Table 7
Emission and excitation data for selected $(AuX)_n(\mu\text{-dpep})_n$ (X = Cl, Br, and I; n = 2, 3, and 4) compounds [43][a].

Compound	278 K		77 K	
	Excitation (nm)	Emission (nm)	Excitation (nm)	Emission (nm)
dpep	275–300	423	250–300	423
$[Au_2(\mu\text{-dpep})_2]Cl_2{\cdot}2CHCl_3$	285	518	354	504
$[Au_2(\mu\text{-dpep})_2]Br_2$	280–340	527	280–325	495
$[Au_2(\mu\text{-dpep})_2]I_2$	342	475(sh), 513	280–325	455
$[(\mu\text{-dpep})(AuCl)_3]{\cdot}3CH_2Cl_2$	352	482, 530(sh)	333	469
$[(\mu\text{-dpep})(AuBr)_3]$	379	506	354	495
$[(\mu\text{-dpep})(AuI)_3]$	324, 368	537	330, 375	563
			341	460(sh), 562
$[(\mu\text{-dpep})(AuBr)_4]$	310–360, 380	521, 580(sh)	362	509
$[(\mu\text{-dpep})(AuI)_4]$	–	–	354	473

[a] dpep = tris[2-(diphenylphosphino)ethyl]phosphine.

Trinuclear phosphinegold(I) halides also present interesting molecular structures with aurophilic interactions. Two views of the molecular structure of $HC[PPh_2(AuCl)]_3$ are shown in Fig. 8; the molecule has crystallographic threefold symmetry [38]. The characteristic linear coordination geometry is found for gold, and chloride atoms are splayed out with respect to the Au_3 triangle (Fig. 8b); see Table 5 for key bond distances for this and the isomorphous iodide structure [36]. While the former phosphine gives rise to structures similar to a first approximation to the monomeric species described in Section 2, the disposition of the phosphine donor atoms is tuned to facilitate the formation of aurophilic interactions that were absent in some of the monomeric species. In the same way, a related tridentate ligand, bis(diphenylphosphinomethyl)phenylphosphine (dpmp), generates structures clearly related to those formed by the dcpm and dppm phosphines ligand but with two eight-membered $[Au–P–C–P]_2$ rings fused leading to a three-membered chain of gold atoms akin to that observed in the crystal structure of $\{(Me_2PhP)AuCl\}_3$ (Fig. 3). The prototype monocationic structure, i.e. $[Au_3(\mu\text{-dpmp})_2Cl_2]^+$ [36], is illustrated in Fig. 9a and Au. . .Au distances are listed in Table 5. In the monocation, each of the exocyclic gold atoms carries a chloride atom. The two Au–Cl distances are 2.770(12) and 2.844(13) Å. The longer of these

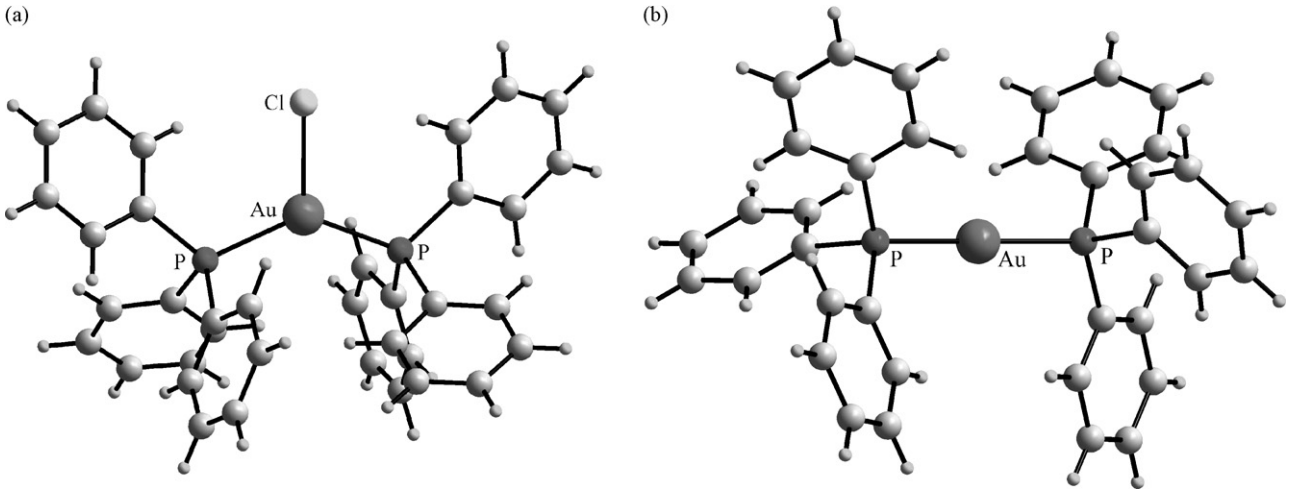

Fig. 13. Molecular structures of (a) neutral and trigonal planar $[Au(PPh_3)_2Cl]$, being representative of the $[Au(PPh_3)_2X]$ compounds; and (b) the linear monocation in $[Au(PPh_3)_2]PF_6$ [48].

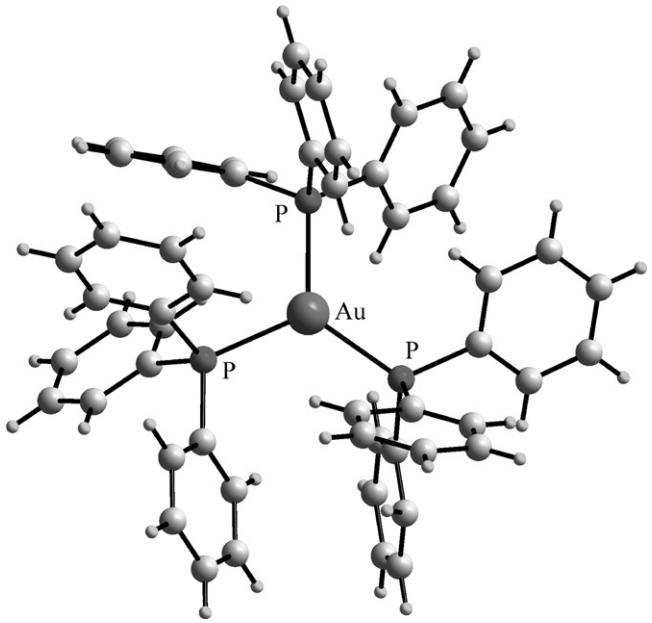

Fig. 14. Molecular structure of the trigonal planar cation in $[Au(PPh_3)_3]BPh_4$ [49].

distances is formed by the chloride atom orientated over the central gold atom [Au–Cl 3.286(12) Å]. The Au–Cl bond distances in $[Au_3(\mu\text{-dpmp})_2Cl_2]^+$ are considerably longer than 2.278(1) Å in the structure of Ph_3AuCl [17] and 2.300(5) Å in $HC[PPh_2(AuCl)]_3$ [38]. Not surprisingly, the Au. . .Au distances concomitantly increase in significance (Table 5). A structural change occurs in the dicationic species, $[Au_3(\mu\text{-dpmp})_2Cl](PF_6)_2$ [39], as shown in Fig. 9b. Here, the chloride atom is coordinated to the central gold atom [2.929(6) Å] but, at the same time forms a weak interaction to one of the exocyclic gold atoms [3.219(7) Å]. Despite the changes in charge and structure, the magnitudes of the Au. . .Au separations are to a first approximation the same. This observation is reflected in their luminescence behavior.

The $[Au_3(\mu\text{-dpmp})_2X_2]^+$, for X = Cl and I [36], compounds demonstrate high- and/or low-energy emissions, as summarized in Table 5. In the solid-state, the high-energy emission maxima are observed in the region 480–575 nm and, when observed, the low-energy emission maxima lie between 620 and 680 nm. The decay times of the compounds in degassed dichloromethane solution are in the range 1.2–2.5 μs. The intensities of the two emission bands are very dependent on the temperature. The low-energy emission gained in intensity with increasing temperature. Other spectroscopic features of note include a small blue-shift in energy on going from iodide to chloride and the observation that the excitation spectra of the high- and low-energy emissions are the same, matching the absorption spectra of the compounds. According to extended-Hückel molecular orbital (EHMO) calculations, for the chloride compounds the main components of the HOMO's and LUMO's correspond to the d orbitals of gold (≈96%) and the phosphine ligand (≈100%), respectively. By contrast, for the iodide compounds the HOMO's have as their main contribution iodide 6p orbitals (>74%) with a smaller contribution from the d orbital of gold (<25%). Based on the above, it was concluded that for the chloride compounds, the excited states for the low-energy emissions arose from the Au(d) → phosphine(π^*) transition. In the iodide compounds, the excited states were associated primarily with I^- → phosphine(π^*) with a contribution from Au(d) → phosphine(π^*). The Au(d) → phosphine(π^*) transition was modified by aurophilic interactions. Consequently, the origin of the low-energy emissions is due to mixed ^{3}MMLCT (gold → phosphine) and/or ^{3}LLCT (iodide → phosphine) transitions. The excited states for the high-energy emissions were assigned as intra-ligand (IL) and ^{3}MLCT (Au(d) → phosphine(π^*)) transitions. The effects of coordinated halide ions on luminescence properties were also observed in the trinuclear dicationic $[Au_3(\mu\text{-dpmp})_2X](PF_6)_2$, X = Cl, Br and I compounds [39]. As noted above, there are no significant variations in the Au. . .Au separations, Table 5. However, in dichloromethane solution the X = Cl compound produced only a high-energy emission, while the iodide compound produced a low-energy emission as the main band and the high-energy emission as a shoulder. Unexpectedly, the bromide compound was almost non-luminescent. The above suggests that in solution, the nature of the halide anion plays a key role in determining the luminescence properties of these compounds. A consideration of the following series of molecules also serves to illustrate this key conclusion.

The potentially tridentate ligand triphos, bis(diphenylphosphinoethyl)phenylphosphine, is related to the previously

Table 8
Emission and excitation data for selected three-coordinate phosphinegold(I) compounds in the solid-state.

Compound	Excitation (nm)	Emission (nm)/lifetime (μs)	Ref.
$[Au(PPh_3)_2Cl]$		540[a]	[50]
$[Au(PPh_3)_2Br]$		530[a]	[50]
$[Au(PPh_3)_2I]$		450[a]	[50]
$[Au(PPh_3)_2]PF_6$	325–380	493/8[b]	[51]
$[Au(PPh_3)_3]BPh_4$	325–380	481/9.3[b]	[51]
$[Au(PPh_3)_3]^+$[c]	325–380	512/10[b]	[51]

[a] 78 K.
[b] 298 K.
[c] Recorded in acetonitrile solution.

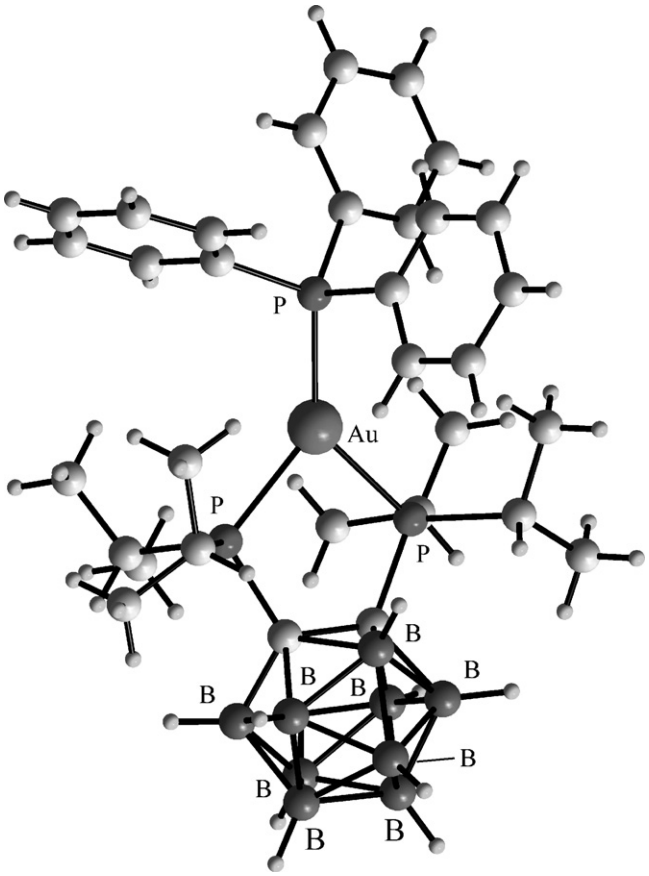

Fig. 15. Molecular structure of $[Au(dipnc)(PPh_3)]$ [55] highlighting the trigonal planar coordination geometry.

Table 9
Excitation and emission peak positions for selected nido-diphosphines and phosphinegold(I) nido-compounds [55].

	In $(CH_3)_2CO$ solution[a]		Solid-state at 77 K	
	Excitation (nm)	Emission (nm)	Excitation (nm)	Emission (nm)
NBu_4(dppnc)[b]	379	429	332	465
[Au(dppnc)(PPh_3)]	338	528	332	529
	453	603	460	676
[Au(dppnc)(PPh_2Me)]	338	530	335	513
	423	576	412	653
[Au(dppnc){P(4-$MeC_6H_4)_3$}]	396	534	337	506
			459	633
NBu_4(dipnc)[c]	340	422	335	488
[Au(dipnc)(PPh_3)]	331	514	337	507
[Au(dipnc)(PPh_2Me)]	338	512	327	505
[Au(dipnc){P(4-$MeC_6H_4)_3$}]	336	512	322	503

[a] Concentration = 2×10^{-3} M.
[b] dppnc = $[(PPh_2)_2C_2B_9H_{10}]^-$.
[c] dipnc = $[(P^iPr_2)_2C_2B_9H_{10}]^-$.

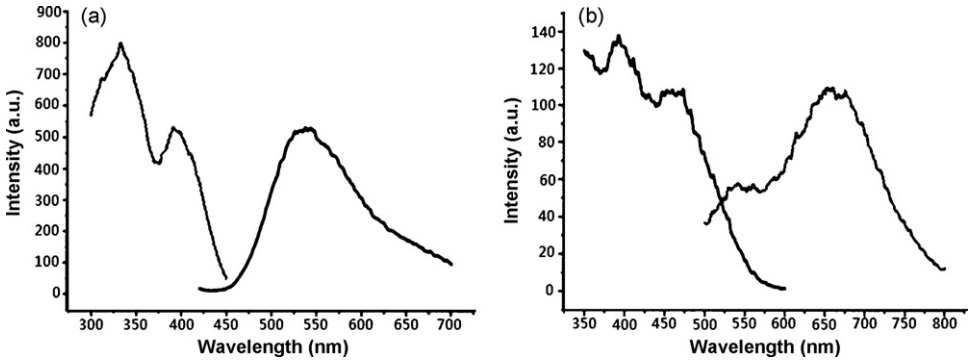

Fig. 16. Emission and excitation spectra for [Au(dppnc)(PPh_3)] recorded in the solid-state at room temperature for: (a) the high-energy emission; and (b) the low-energy emission. Reprinted with permission from [34]. ©(2003) American Chemical Society.

discussed dpmp phosphine but with ethylene rather than methylene bridges so as to increase the separation between the phosphorus donor atoms. The crystal structure of the trinuclear iodide derivative, [(μ-triphos)$(AuI)_3$], is available and is represented in Fig. 10 [40]; the molecule has crystallographic mirror symmetry. The key feature of note in this structure is the absence of Au...Au interactions and so the structure might be thought of being simply a chain of three unconnected P–Au–I units as in the structure of mononuclear Ph_3PAuI [18a,19]. Consistent with this assignment is that the Au–P [2.252(3)–2.258(4) Å] and Au–I

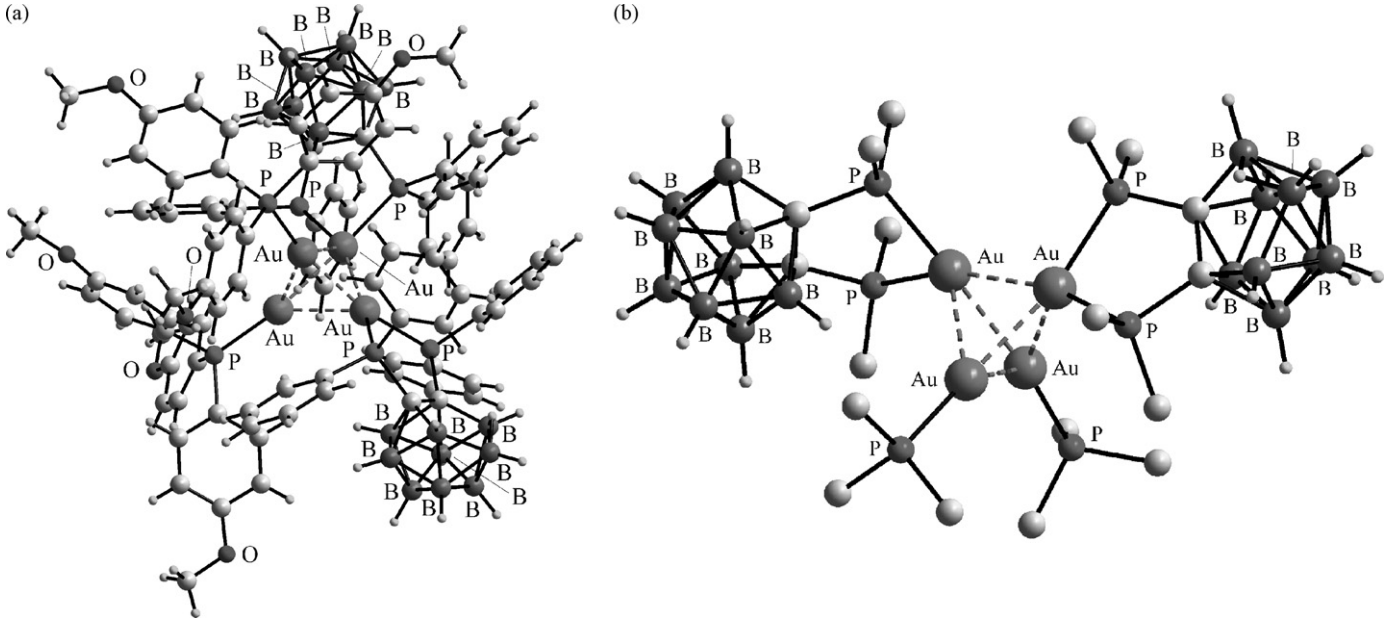

Fig. 17. Molecular structure of: (a) the tetranuclear [Au_4{dppnc}$_2$(P(C_6H_4OMe-4)$_3$)$_2$] [54]; and (b) a simplified view of [Au_4{dppnc}$_2$(P(C_6H_4OMe-4)$_3$)$_2$] [54] showing only ipso-carbon atoms of the phenyl rings and with most hydrogen atoms omitted for clarity; aurophilic interactions are represented by dashed lines.

[2.5610(15)–2.5742(11) Å] bond distances are comparable to those observed in Ph_3PAuI, i.e. 2.254(4) and 2.5555(16) Å, respectively [18a,19].

Laguna and co-workers reported optical properties for a series of trinuclear gold(I) compounds [(μ-triphos)$(AuX)_3$], X = Cl, Br, I, and C_6F_5, see Table 6 [41]. At room temperature, tripos and the X = Br and I compounds show luminescence, peaking at 425, 475 and 525 nm, respectively, while the X = Cl and C_6F_5 compounds are not luminescent. At 77 K, all four compounds are luminescent, significantly more intense than the free ligand. As can be seen from the data included in Table 6, the luminescence properties are significantly influenced by the halide anions. These results indicate that the contribution of the respective halides to the energy levels is very important as noted earlier for the binuclear gold(I) derivatives.

The potentially tetradentate phosphine ligand tris[2-(diphenylphosphino)ethyl]phosphine (dpep) forms di-, tri- and tetra-nuclear compounds, many of which exhibit luminescence [42,43]. A representation of the molecular structure of the dication in $[(\mu\text{-dpep})_2Au_2]Cl_2\cdot 2CHCl_3$ [42] is shown in Fig. 11a and b. Here, the two dpep molecules bridge two gold centers employing all possible phosphorus donors leading to heavily distorted tetrahedral coordination geometries. While definitive structural data are not available for the trinuclear [(μ-dpep)$(AuX)_3$] species, it is likely to resemble the structure of [(μ-triphos)$(AuI)_3$] (Fig. 10) [40]. A crystal structure determination has been reported for [(μ-dpmp)$(AuBr)_4$] [42]. As shown in Fig. 11c and d, each of the four phosphorus donors atoms is coordinated to a AuCl residue and two tetranuclear species associate via a Au. . .Au interaction [3.061(5) Å]. The observed optical properties measured at 278 and 77 K are shown in Fig. 12 and data are summarized in Table 7 [43]. The emission intensity and energy of the binuclear $[(\mu\text{-dpep})_2Au_2]X_2$ compounds at 77 K increase from Cl to Br to I. Taking into account that there are no Au. . .Au interactions of note, assuming the X = Br and I structures resemble that for the X = Cl compound (Fig. 11a), the significant influence on the emissions from $[(\mu\text{-dpep})_2Au_2]X_2$ arises from the halide counter anion as described above for $[(\mu\text{-dcpm})_2Au_2]X_2$. As halide is varied, systematic changes were also found in the emission intensity and energy. For the [(μ-dpep)$(AuX)_3$] and [(μ-dpep)$(AuX)_4$] compounds, the emission energy decreases from X = Cl to Br to I (Table 7); n.b. the [(μ-dpep)$(AuCl)_4$] species was non-emissive. These results suggest that the halide, either as a counter anion or as a ligand, can influence the energy levels of the emitting center.

4. Three coordinate phosphinegold(I) compounds

Three-coordinate phosphinegold(I) compounds are luminescent in solution and in the solid-state. All structures present steric crowding and no aurophilic interactions are noted in their crystal structures. Compounds of the general formula $[Au(PPh_3)_2X]$ present different coordination geometries depending on the nature of the counter-ion. When X = Cl, a tri-coordinate, trigonal planar gold atom is observed in the crystal structure (Fig. 13a) [44]. The Au–Cl [2.533(4) Å] and Au–P [2.316(4) and 2.336(4) Å] bond distances fall in the range of Au–Cl [2.500(4)–2.5768(6) Å] and Au–P [2.3134(16)–2.3464(6) Å] distances in the hemi-benzene [45], chloroform [46], and dichloromethane [47] solvates of $[Au(PPh_3)_2Cl]$. The P–Au–P angle in all four structures lies in the narrow range 132.1(1)–136.05(19)°. The $[Au(PPh_3)_2X]$, X = Br and I, compounds are isomorphous, have crystallographic twofold symmetry and adopt structures as for the X = Cl derivative with experimentally equivalent Au–P bond distances and the expected elongation in Au–X [44]. The structure of the $X = PF_6$ species [48] presents a distinct structural form as the anion is non-coordinating (Fig. 13b). The coordination geometry about the gold atom is linear [177.4(1)°]

Table 10
Luminescence properties of selected dinuclear phosphinegold(I) thiolates in the solid-state measured at room temperature [59][a].

Compound	Au. . .Au (Å)[b,c]	Excitation (nm)	Emission (nm)
[(μ-dppe)$(Au(p\text{-}tc))_2$]		380	495
[(μ-dppp)$(Au(p\text{-}tc))_2$]	3.13	380	485
[(μ-dppb)$(Au(p\text{-}tc))_2$]	3.08 [3.094(1)]	380	485
[(μ-dpppn)$(Au(p\text{-}tc))_2$]	3.10 [3.200(1)]	375	485
[(μ-dppe)(Au_2pdt)]	2.96	390	515
[(μ-dppp)(Au_2pdt)]	2.93	380	500
[(μ-dppb)(Au_2pdt)]		395	510
[(μ-dpppn)(Au_2pdt)]		390	505
[(μ-dcpe)$(Au(p\text{-}tc))_2$]		380	495

[a] p-tc is the anion derived from p-thiocresol; pdt is the anion derived from 1,3-propanedithiol; dcpe is 1,2-bis(dicyclohexylphosphino)ethane; dppe is $Ph_2P(CH_2)_nPPh_2$ for $n = 2$, for $n = 3$ dppp, $n = 4$ dppb, and $n = 5$ dpppn.
[b] Au. . .Au distances determined from EXAFS.
[c] Au. . .Au in square brackets determined by X-ray crystallography.

with Au–P [2.309(3) and 2.313(3) Å], i.e. at the lower end of the range of Au–P bond distances for the aforementioned structures. A three-coordinate, trigonal planar geometry is found for the triphosphinegold(I) cation in $[Au(PPh_3)_3]BPh_4$ (Fig. 14) [49].

As summarized in Table 8, the three-coordinate phosphinegold(I) compounds, when excited in the UV region, produced a single emission band in the range 450–540 nm [50–52]. These emissions have been attributed to a metal-centered $^3[p_z \rightarrow d_{x2-y2}, d_{xy})]$ transition. For the $[Au(PPh_3)_2X]$ compounds, the emission undergoes a blue-shift as the halide varies Cl to Br to I. DFT calculations for $[Au(PPh_3)_2Cl]$ revealed that upon excitation the geometry dramatically changes in the excited state [50]. It indicates that the steric crowding in the three-coordinate excited state may be significant in determining the emission energy [50,52].

Finally, the structural and optical properties of multi-coordinate gold(I) compounds with carborane-diphosphines have been extensively investigated [53–56] with both closo- and nido-carborane diphosphine derivatives forming very stable gold species. Representative crystal structures are available. The molecular structure of [Au(dipnc)(PPh_3)] [55], where dipnc is the uninegative anion, bis(diisopropylphosphine) nido-carborane $[(P^iPr_2)_2C_2B_9H_{10}]^-$, features an approximately trigonal planar coordination geometry for gold (Fig. 15) and is therefore closely related to the cationic structure shown in $[Au(PPh_3)_3]BPh_4$ [49] (Fig. 14). In the neutral structure, the Au–P bond distances formed by the dipnc anion [2.3790(6) and 2.4083(6) Å] are significantly longer than that formed by neutral Ph_3P [2.3077(6) Å]. A similar coordination geometry and pattern of bond distances occurs in the structure of [Au(dppnc)(PPh_3)] [53], where dppnc is bis(diphenylphosphine) nido-caborane.

The nido-diphosphine derivatives $[(PR_2)_2C_2B_9H_{10}]_2^-$ ($R = PPh_2$, P^iPr_2), both in solution and in the solid-state are luminescent, while the neutral closo-diphosphines display no luminescence. This observation indicates that the radiative transitions of the substituted diphosphines are most likely associated with the orbitals of the carborane cage. From the data collated in Table 9, the three-coordinated dppnc gold(I) compounds produce two emission bands at 77 K: the high- and low-energy emission bands are located in the 506–529 and 633–676 nm regions, respectively. By contrast, each of the gold(I) compounds with dipnc show only a high-energy band located in the region 503–507 nm. The similarity in the excitation and the red-shifted emission to those of the uncoordinated dipnc ligand supports the attribution of the high-energy emission to the carborane cage intra-ligand transitions perturbed by the gold atom. As shown in Fig. 16 for [Au(dppnc)(PPh_3)], the excitation spectrum of the low-energy emission is different from that of the high-energy emission, indicating that the two emitting centers are different. It is apparent, Table 9, that the low-energy emission is very dependent on the nature of the monodentate phosphine bound to the

gold as the emission peak is blue-shifted as the phosphine varies from PPh_3 to PPh_2Me to $P(4\text{-}MeC_6H_4)_3$. This behavior is in accordance with the π-acceptor ability of the phosphines that varies, i.e. $PPh_3 > PPh_2Me > P(4\text{-}MeC_6H_4)_3$ [57]. These spectroscopic features suggest that the low-energy emission be assigned as arising from a MLCT [Au → π*(L)] excited state.

Tetranuclear gold clusters $[Au_4\{dppnc\}_2(PR_3)_2]$ have been prepared from nido-carborane diphosphine and PR_3 [54,56]. Two views of a representative structure, namely $[Au_4\{dppnc\}_2(P(C_6H_4OMe\text{-}4)_3)_2]$ [54], are shown in Fig. 17. The neutral structure is constructed about a tetrahedral core of gold atoms linked by Au...Au contacts. Formally, two of the gold atoms are in the +I oxidation state leaving two gold(0) centers. The two gold atoms coordinated by the monodentate $P(C_6H_4OMe\text{-}4)_3$ ligands are assigned as gold(I); the assignment was supported by MP2 calculations [54]. The Au...Au separations range from 2.630(3) to 2.872(2) Å and the pattern of Au–P bond distances resembles that outlined above for the structure of [Au(dipnc)(PPh_3)] [55]. The tetranuclear compounds when excited at approximately 390 nm produced only low-energy emissions.

5. Phosphinegold(I) thiolates

Most phosphinegold(I) thiolates exhibit luminescence in both in solution and in the solid-state. It is also well established that their visible luminescence properties are significantly influenced by the nature of the thiolate ligands when they contain a chromophore.

Elder, Bruce, Bruce and co-workers investigated several series of neutral, dinuclear diphosphinegold(I) thiolate compounds in which the phosphine ligands have various spacers between the phosphorus donor atoms and the thiolates are derived p-thiocresol and 1,3-propanedithiol [58,59]. Two X-ray crystal structures are available for these series, namely [(μ-dppb)(Au(p-tc))$_2$] (Fig. 18a) and [(μ-dpppn)(Au(p-tc))$_2$] [59]. Both structures adopt an open configuration with respect to the diphosphine ligand and an anti-disposition of the gold(I)thiolate residues; the dppb molecule is disposed about a center of inversion. The coordination for gold is linear within a SP donor set. As for all related compounds, the Au–S bond distance [2.306(3) Å] is longer than the Au–P distance [2.263(2) Å]; the P–Au–S angle is 172.96(8)°. The crystal packing in each compound presents supramolecular chains mediated by Au...Au interactions; see Table 10 for data. The dppb species (Fig. 18b) has a more compact arrangement compared with the "head-to-tail" pattern observed for the dpppn structure (Fig. 18c). The magnitudes of the Au...Au distances determined by X-ray crystallography mirror the values determined by EXAFS [59], Table 10. When dissolved in methylenechloride solution, most of the compounds show three to six absorption bands with peaks in the range 350–260 nm. The two lowest-energy bands appeared below 300 nm and were assigned as LMCTs (S → Au). As summarized in Table 10,

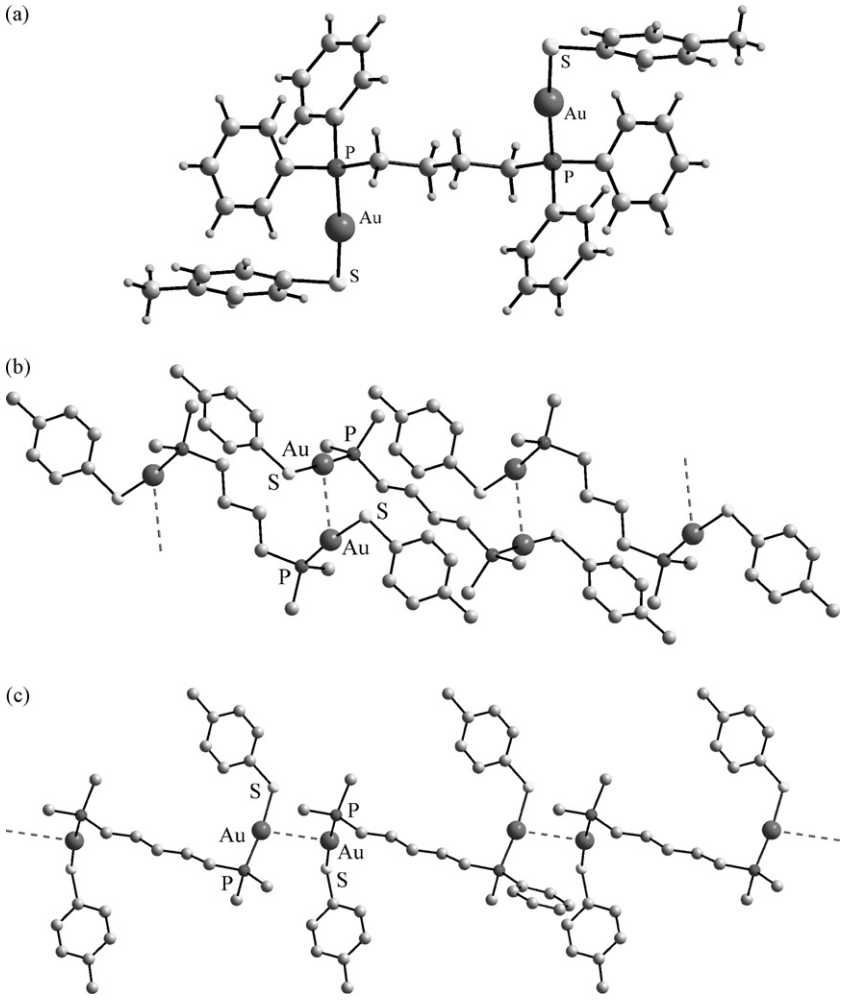

Fig. 18. (a) Molecular structure of dinuclear [(μ-dppb)(Au(p-tc))$_2$] [59]; (b) supramolecular aggregation in [(μ-dppb)(Au(p-tc))$_2$] [59] mediated by aurophilic interactions; and (c) "head-to-tail" supramolecular aggregation in [(μ-dpppn)(Au(p-tc))$_2$] [59] mediated by aurophilic interactions. In (b) and (c), the phosphorus-bound phenyl rings are indicated by the ipso-carbon atoms and all hydrogen atoms have been removed for clarity; aurophilic interactions are represented by dashed lines.

Table 11
Luminescence and lifetime data for selected [(Ph_3P)AuSR] and [(TPA)AuSR], SR = benzenethiolate derivative, data collected at 77 K [60].

Compound	Au. . .Au (Å)	Excitation (nm)	Emission (nm)	Lifetime (μs)
$Ph_3PAuSPh$	3.155(2)[a]	360	413	17 + short component
$Ph_3PAuS(C_6H_4OMe\text{-}2)$	None[a]	350	429	75, 0.013
$Ph_3PAuS(C_6H_4Cl\text{-}2)$	None	317	461	1.89 + short component
(TPA)AuSPh	None	358	596	8
$(TPA)AuS(C_6H_4OMe\text{-}2)$	3.2632(14), 3.3406(16)	365	589	11
$(TPA)AuS(C_6H_4OMe\text{-}3)$		368	685	15
$(TPA)AuS(C_6H_4Cl\text{-}2)$		363	540	217
$(TPA)AuS(C_6H_4Cl\text{-}3)$		365	702	15
$(TPA)AuS(C_6H_4Cl\text{-}4)$		362	698	16
$(TPA)AuS(C_6H_3Cl_2\text{-}3,5)$	3.047(3)	366	485	6
$(TPA)AuSCH(CH_3)_2$		348	669	17

[a] Au. . .Au distances extracted from Ref. [61].

Table 12
Absorption data for $(o\text{-tolyl})_3P$, 2-HmbaH, and $(o\text{-tol})_3PAu(2\text{-mbaH}).EtOH$ [64].

Compound	λ_{max}/nm (ε/M^{-1} cm^{-1})	Main transition
$(o\text{-tolyl})_3P$	274 (47,570)	$\pi \rightarrow \pi^*$
	233 (30,580)	$\pi \rightarrow \pi^*$
2-HmbaH	302 (5,240)	$n(S,O) \rightarrow \pi^*(HmbaH)$
	249 (23,100)	$\pi(S\text{-}HmbaH) + \pi(HmbaH) \rightarrow \pi^*(mbaH)$
	228 (22,720)	$\pi(S\text{-}mbaH) \rightarrow \pi^*(mbaH)$
$(o\text{-tolyl})_3PAu(2\text{-mbaH}).EtOH$	311 (3,690)	$\pi(S\text{-}mbaH) \rightarrow \pi^*(Au)$
	280 (2,530)	$\pi(S\text{-}mbaH) \rightarrow \pi^*(Au)$
	271 (1,560)	$\pi(S\text{-}mbaH) \rightarrow \pi^*(Au)$
	244 (37,750)	$\pi(S\text{-}mbaH) \rightarrow \sigma^*(S\text{–}Au\text{–}P)$
	227 (33,960)	$\sigma(Au\text{–}P) \rightarrow \pi^*(Au)$

the emission maxima of the thiolate compounds are very similar, appearing in the range of 485–510 nm. Their excitation bands correspond to the lowest absorption bands. The data suggest that no correlation exists between the magnitude of the Au. . .Au distance and the observed emission energy. These results provide support that the observed luminescence originates from the S → Au charge transfer excitation.

Fackler and co-workers [60] investigated the effect upon luminescence properties of introducing systematic variations in the benzenethiolate ligand and by changing the phosphine ligand. A total of six different crystal structures are available for the compounds listed in Table 11. The common feature of the structures is the linear SP coordination geometry for gold and the same pattern in bond distances as for [(μ-dppb)(Au(p-tc))$_2$] [59]. Thus, for the Ph_3P series, the Au–S bond distances lie in the range 2.292(2)–2.324(2) Å, Au–P 2.255(2)–2.282(2) Å, and P–Au–S 173.11(6)–179.0(1)°. The structure of $Ph_3PAuSPh$ (Fig. 19a) highlights the linear coordination geometry for gold and shows dimerization via the formation of an Au. . .Au interaction [61]. The two other Ph_3P structures, i.e. $Ph_3PAuS(C_6H_4OMe\text{-}2)$ [61] and $Ph_3PAuS(C_6H_4Cl\text{-}2)$ [60], do not feature aurophilic interactions. The geometric parameters for $Ph_3PAuSPh$ fall within the cited ranges for all three Ph_3P structures indicating no influence exerted on these by the Au. . .Au contact. In the three examples where the phosphine ligand is 1,3,5-triaza-7-phospha-adamantane (TPA) an intriguing observation is made. In the case where the thiolate ligand is thio-

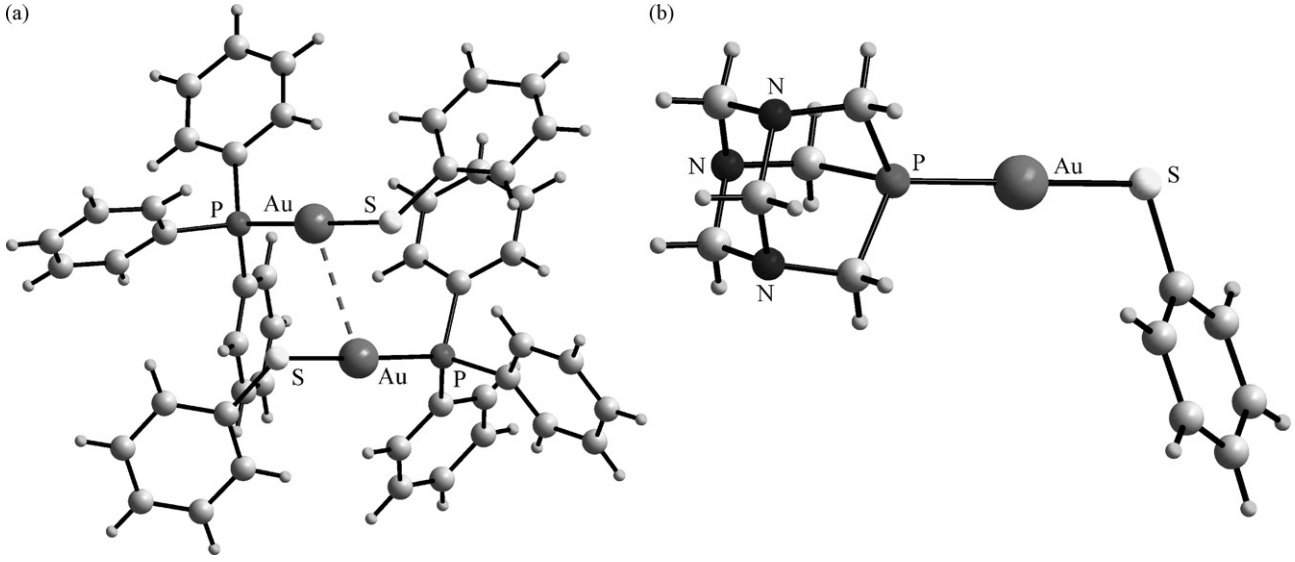

Fig. 19. (a) Supramolecular aggregation mediated by an Au. . .Au interaction in the structure of $Ph_3PAuSPh$ [61], featuring a linear P–Au–S coordination geometry; and (b) molecular structure of (TPA)AuSPh [60]; aurophilic interactions are represented by dashed lines.

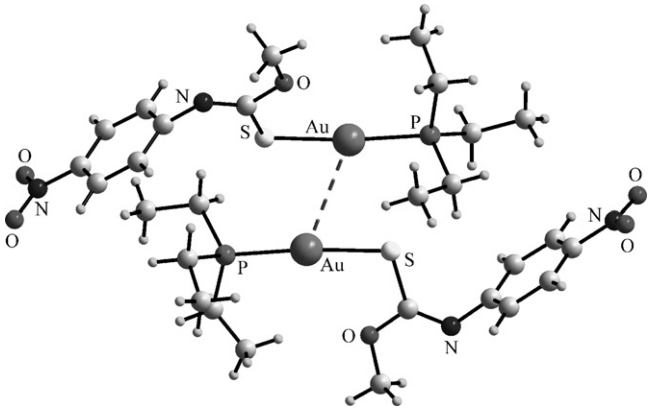

Fig. 20. Supramolecular aggregation mediated by an Au. . .Au interaction in the structure of [$Et_3PAu\{SC(OMe)=NC_6H_4NO_2\text{-}4\}$] [62]; aurophilic interactions are represented by dashed lines.

phenolate, an aurophilic interaction is not found in the structure of (TPA)AuSPh (Fig. 19b) whereas for the Ph_3P derivative, such a contact was formed. However, the reverse trend is evident when the thiolate ligand is $AuS(C_6H_4OMe\text{-}2)$. Not surprisingly, there are no systematic variations in the Au–S, Au–P and P–Au–P geometric parameters. In terms of luminescence, the emission maxima are over a relatively wide range of 413–700 nm and there is no obvious correlation between the Au. . .Au distance and the emission energy. For the TPA compounds, the excitation is associated with the thiolate ligands, since TPA shows no absorption band above 210 nm. The observed luminescence properties of the compounds originate from the S → Au charge transfer excited states. As suggested in the original study [60], the variation of the emission band could be associated with the electron-withdrawing groups on the thiolate ligand.

In a systematic study of mononuclear [$R_3PAu\{SC(OMe)=NC_6H_4NO_2\text{-}4\}$], for R = Et, Cy, and Ph, and binuclear [$(Ph_2P(CH_2)_nPPh_2)\{Au\{SC(OMe)=NC_6H_4NO_2\text{-}4\}_2$], for n = 1–4, the effect upon luminescence properties by systematically varying the phosphine ligand was investigated [62]. When excited at 380–387 nm all compounds, both in solution and in the solid-state, produced a single emission band. In the solid-state, at 77 K, a small blue-shift was observed for the emission peak, i.e. from 538 to 526 to 517 nm for R = Et to Cy to Ph, respectively, while for binuclear phosphines, the positions of the emission peaks were almost independent on the length of alky chain, i.e. λ_{ems} = 541, 541, 543 and 547 nm for n = 1, 2, 3 and 4, respectively [62]. In the mononuclear compounds, the smaller R = ethyl substituent in [$Et_3PAu\{SC(OMe)=NC_6H_4NO_2\text{-}4\}$] allows for the formation supramolecular association via an Au. . .Au [3.6086(3) Å] interaction (Fig. 20) that are absent for substituents R = Cy and Ph. This systematic study indicates that the excitation and emission maxima are almost independent of the nature of the ancillary phosphines, and whether an Au. . .Au interaction, either inter- or intra-molecular, is present or not [62].

In a related study, gold(I) compounds with monodentate $P(CH_2CH_2CN)_3$ or bidentate 1,6-bis(diphenylphosphino)hexane (dpph) of 2-amino-5-mercapto-1,3,4-thiazolate ($SSNH_2$) and 6-amino-2-mercaptobenzothiazole ($SSCNH_2$) were investigated; molecular structures of representative compounds, i.e. $(CH_2CH_2CN)_3PAu(SSNH_2)$ and (μ-dpph)$(AuSSCNH_2)_2$, are shown in Fig. 21 and present the expected features. At 77 K, when excited at 355 nm, these compounds show one or two emission bands in the region 450–750 nm, accompanied by a very weak band at the high-energy side [63]. The strong bands result from S → Au charge transfer and the weak high-energy emission is related to the phosphine ligands. Although most aromatic phosphine ligands are luminescent, their intra-ligand luminescence does not appear or appears only as a trace in the high-energy side, compared with the main emission originated from the S → Au charge transfer.

A recent study investigated the structural and optical properties of (o-tolyl)$_3$PAu(2-mbaH), where 2-mbaH = 2-mercaptobenzoate, which was characterized as four distinct solvates, acetonitrile, dimethylsulfoxide, methanol, and ethanol [64]. The structure of the ethanol solvate is represented in Fig. 22a which highlights the formation of a 16-membered ring mediated by two O–H. . .O and two O–H. . .S hydrogen bonds; the structure of the methanol solvate

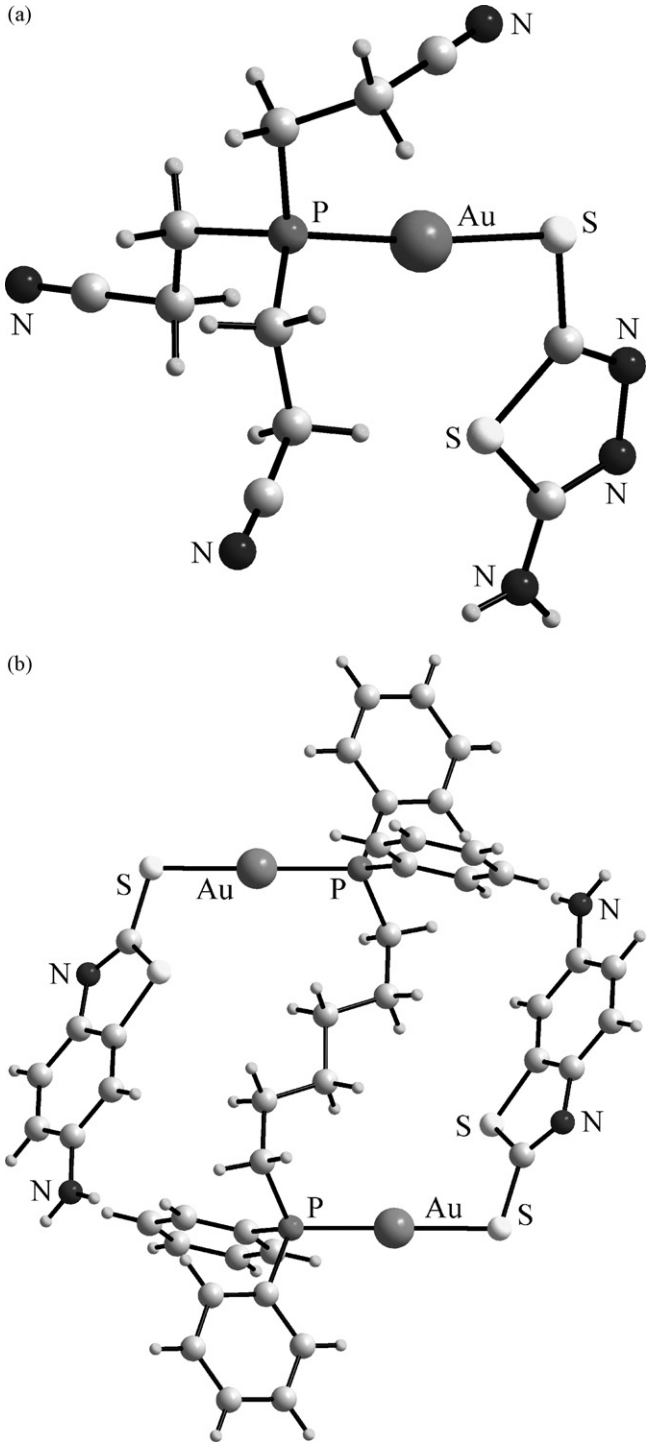

Fig. 21. Molecular structures of: (a) $(NCCH_2CH_2)_3PAu(SSNH_2)$; and (b) dinuclear (μ-dpph)$(AuSSCNH_2)_2$ [63].

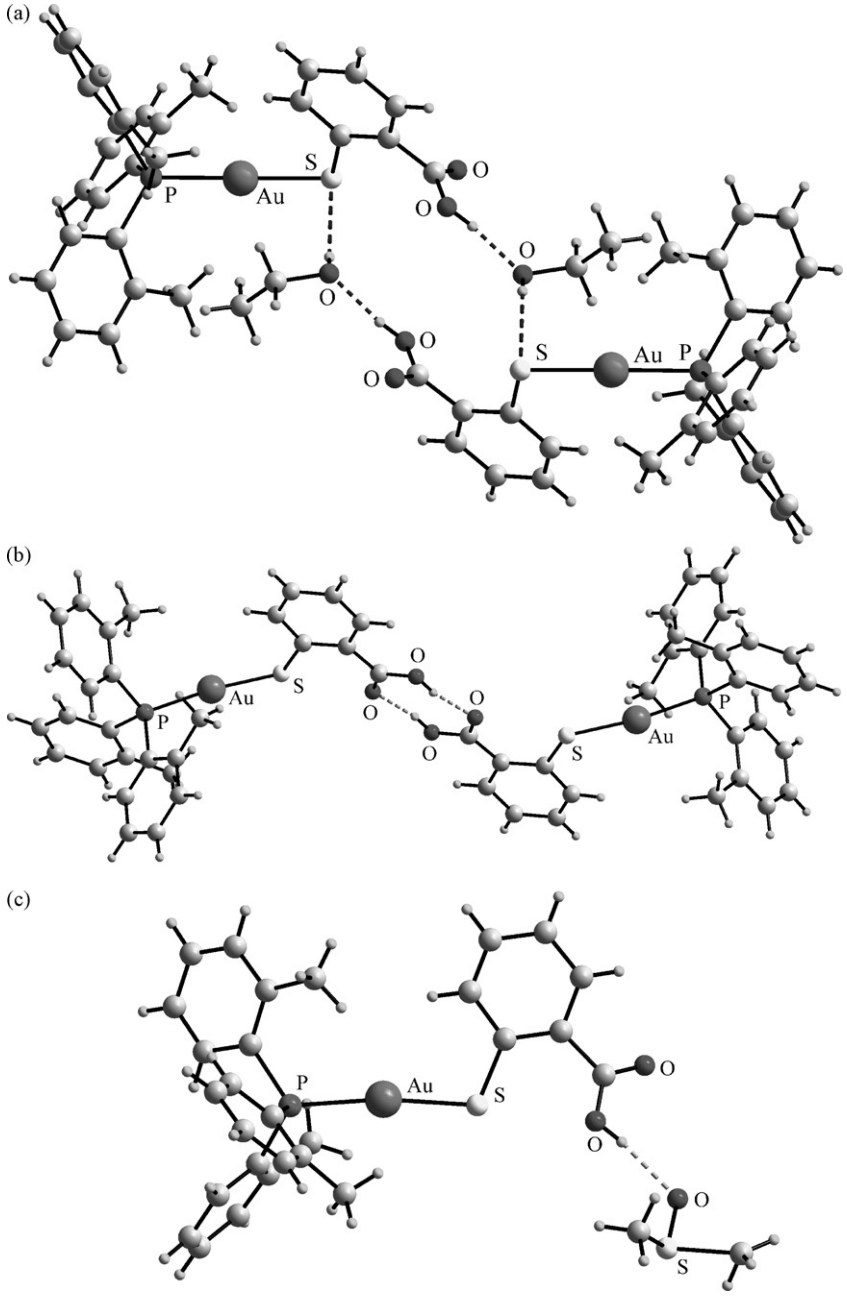

Fig. 22. (a) Supramolecular aggregation mediated by an O–H···O and O–H···S hydrogen bonding in the structure of (o-tolyl)$_3$PAu(2-mbaH).EtOH [64]; (b) dimer formation via the eight-membered $\{\cdots HOC{=}O\cdots\}_2$ carboxylic acid dimer synthon in the structure of (o-tolyl)$_3$PAu(2-mbaH)·CH$_3$CN [64]; and (c) hydrogen bonding between the components of the structure in (o-tolyl)$_3$PAu(2-mbaH)·DMSO [64]; hydrogen bonds are represented by dashed lines.

is isomorphous. With acetonitrile, the familiar eight-membered $\{\ldots HOC{=}O\ldots\}_2$ carboxylic acid dimer synthon is found (Fig. 22b) and when dimethylsulfoxide was the solvent, a O–H. . .O hydrogen bond was formed between the compound and the solvent (Fig. 22c). Regardless of the supramolecular aggregation pattern in force, there were no significant differences in the derived geometric parameters for the different (o-tolyl)$_3$PAu(2-mbaH) molecules. Absorption and emission data for the ethanol solvate are listed in Tables 12 and 13, respectively. The emission intensity of (o-tolyl)$_3$PAu(2-mbaH) was dependent on the nature of the included solvent molecules in the

Table 13
Excitation and emission data for (o-tolyl)$_3$P, 2-HmbaH, and (o-tolyl)$_3$PAu(2-mbaH).EtOH [64].

Compound	Resolved components (nm)	
	Excitation	Emission
(o-tolyl)$_3$P	280(w), [299(w), 319(m),341(p)][a], 369(w)	413(w), 437(s), 467(m)
2-HmbaH	367(m), [384(p), 403(p), 422(p)]a, 451(p)	447(w), [404(p), 489(p), 512(m)][a], 539(m), 579(w), 613(vw)
(o-tolyl)$_3$PAu(2-mbaH)·EtOH	330(w), 360(p), 385(s)	475(m), 512(p), 576(m)

[a] Multiple components are due to the vibronic distortion.

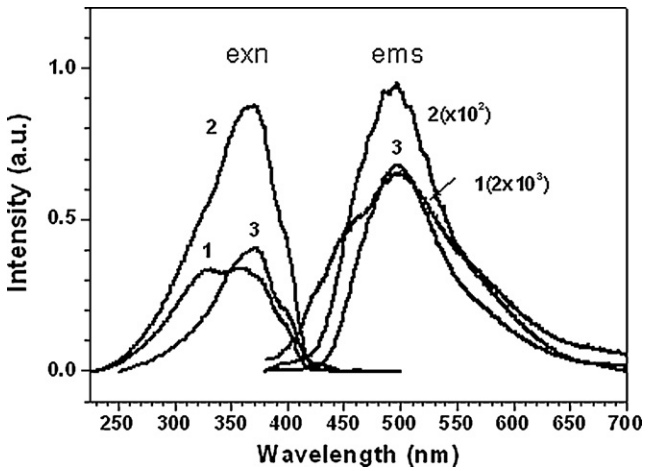

Fig. 23. Emission spectra of (o-tolyl)$_3$PAu(2-mbaH) isolated as its acetonitrile (1), dimethylsulfoxide (2) and ethanol (3) solvates, and excitation spectra of the 460 (1), 500 (2) and 560 (3) nm of (o-tolyl)$_3$PAu(2-mbaH)·EtOH. The spectra were recorded in the solid-state at 78 K. Modified with permission from [64]. ©(2006) American Chemical Society.

crystal structure. Luminescence spectra for acetonitrile, dimethylsulfoxide and ethanol solvates (o-tolyl)$_3$PAu(2-mbaH) are shown in Fig. 23. The luminescence intensity of the ethanol solvate was 1500 times greater than that of the acetonitrile solvate and 60 times greater than the dimethylsulfoxide solvate, indicating the influence of solvent upon the coherence of the crystal lattice. The emission spectrum of (o-tolyl)$_3$PAu(2-mbaH) was very broad, appearing in the 450–650 nm region. The band shape is asymmetric and was resolved into three Gaussian components, peaking at 475, 512 and 576 nm for the ethanol adduct. The spectroscopic shape of the high-energy 475 nm excitation band is somewhat different from those of the two low-energy bands, i.e. 512 and 576 nm, as shown in Fig. 23. The observed emission and excitation spectroscopic features of the (o-tolyl)$_3$PAu(2-mbaH) are apparently different from those of the uncoordinated (o-tolyl)$_3$P and 2-HmbaH molecules (Fig. 24). The intensity of the ethanol solvate is more than 100 times greater than those of the free (o-tolyl)$_3$P and 2-HmbaH molecules. The CIS post-Hartree–Fock calculations on the free molecules and (o-tolyl)$_3$PAu(2-mbaH) · EtOH indicated that it was the excited states from transitions from the first three HOMO's to the first LUMO that are responsible for the emitting levels of the observed emissions.

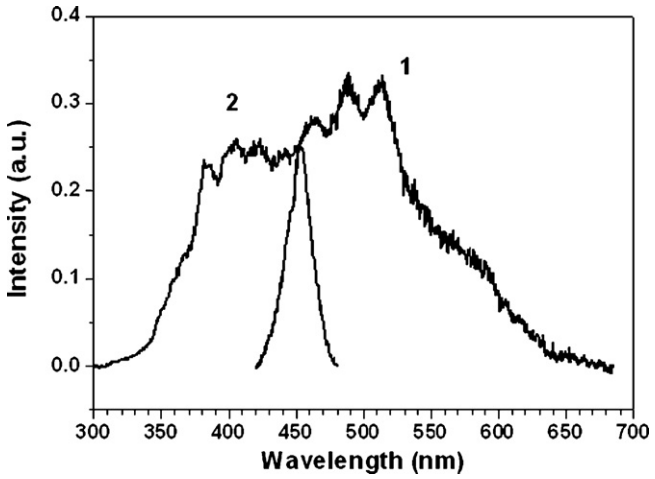

Fig. 24. Luminescence (spectrum 1, λ_{exn} = 400 nm) and excitation (spectrum 2, λ_{ems} = 490 nm) spectra of 2-HmbaH measured in the solid-state at 78.8 K. Reprinted with permission from [64]. ©(2006) American Chemical Society.

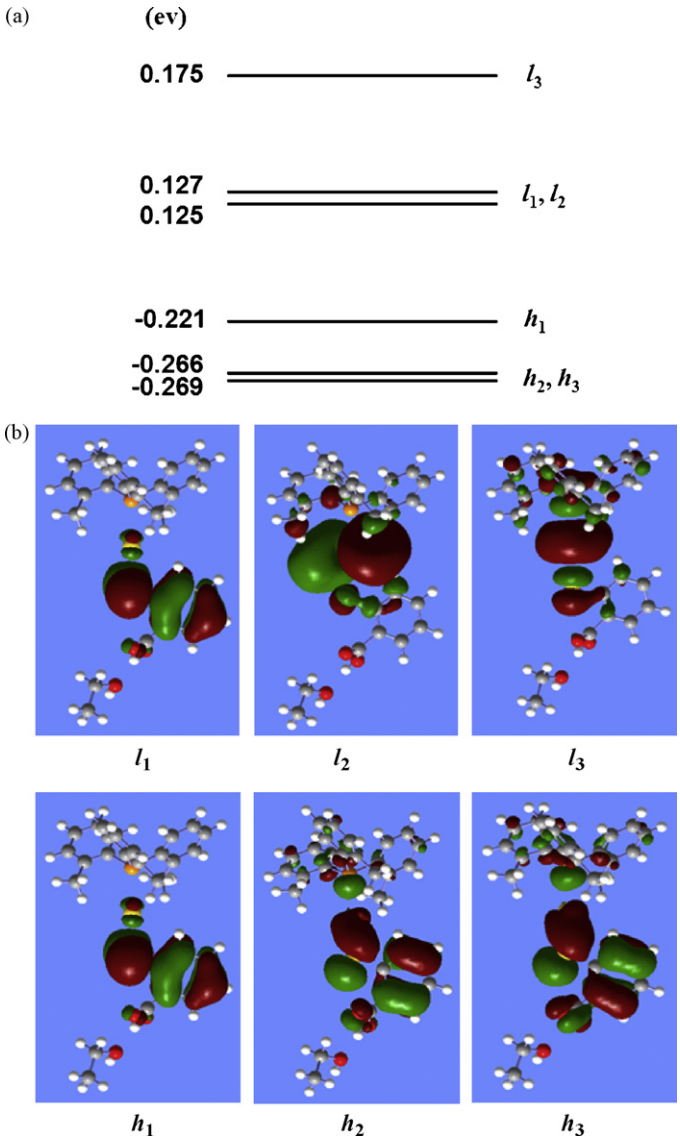

Fig. 25. (a) Energy levels and (b) calculated molecular orbitals for (o-tolyl)$_3$PAu(2-mbaH).EtOH calculated at the level of HF/lan2mz. Reprinted with permission from [64]. ©(2006) American Chemical Society.

As shown in Fig. 25, the non-degenerate *h*1 HOMO corresponds to the linear combination of the p_z orbital of sulfur and the π orbital of the phenyl ring; the molecular axis is along the *x*-axis. The next two *h*2 and *h*3 HOMO's are degenerate, formed from the p_x and p_y of sulfur and the π-system of the phenyl ring. The CIS results and the changes in the electron charges of the constituent atoms suggest that the two low-energy emissions are primarily associated with the $p_z(S) \rightarrow \pi^*(p_z \pm p_y, Au)$ excited states, and that the high-energy emission is primarily associated with the $p_x(S) \rightarrow s(Au)$ excited state. Further, the degenerate excited states responsible for the low-energy emissions are split by the vibronic interaction.

As an extension of these earlier studies, the structural and luminescence properties with supporting *ab* initio molecular orbital calculations were conducted on a series organophosphinegold(I) 2-mercaptobenzamides, $R_3PAu[SC_6H_4C(=O)NH_2\text{-}2]$, R = Et, Ph, and Cy, [65]. In their crystal structures, each compound associates into a centrosymmetric dimer via the eight-membered $\{\ldots HNC{=}O\ldots\}_2$ amide synthon, the R = Et derivative is illustrated in Fig. 26; no significant differences in geometric parameters associated with the

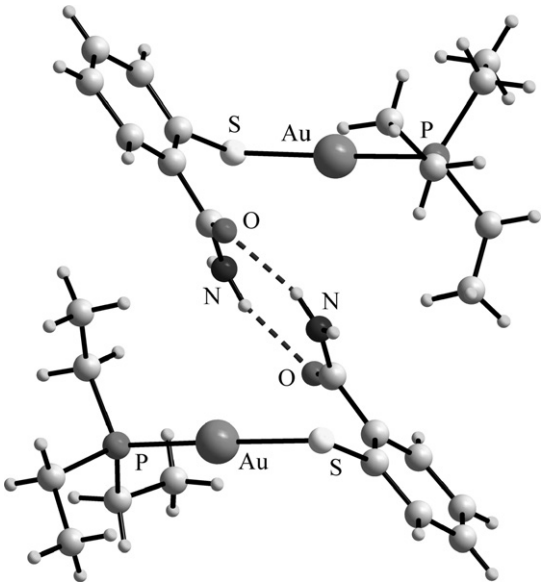

Fig. 26. Dimer formation via the eight-membered $\{\cdots HNC{=}O\cdots\}_2$ amide dimer synthon in the structure of $Et_3PAu[SC_6H_4C(=O)NH_2\text{-}2]$ [65]; hydrogen bonds are represented by dashed lines.

Table 14
Emission and excitation data of selected phosphinegold(I) 2-mercaptobenzamides measured at $T = 10$ K [65].

Compound	Excitation (nm)	Emission (nm)
$Et_3PAu[SC_6H_4C(=O)NH_2\text{-}2]$	324(vb), 356(p)	503(p), 563(sh)
$Ph_3PAu[SC_6H_4C(=O)NH_2\text{-}2]$	321(vb), 356(p)	492(p), 545(sh)
$Cy_3PAu[SC_6H_4C(=O)NH_2\text{-}2]$	310(vb), 365(m), 440(p)	457(m), 503(p), 556(sh)

gold atom in the three structures are apparent. The emission and excitation spectra measured at several temperatures are shown in Fig. 27 and the resolved spectroscopic data are listed in Table 14. The emission and excitation spectra for $Et_3PAu[SC_6H_4C(=O)NH_2\text{-}2]$ are very similar to those of $Ph_3PAu[SC_6H_4C(=O)NH_2\text{-}2]$. The emission spectrum of each compound comprises a main component and a low-energy shoulder. The excitation spectra of the main band and the low-energy shoulder are similar, and both are resolved into a sharpened peak and a broad band at the high-energy side with a trace of a low-energy shoulder. By contrast, the emission spectrum of $Cy_3PAu[SC_6H_4C(=O)NH_2\text{-}2]$ is very different and is dependent on temperature as shown in Fig. 27e. The spectrum at 78 K is resolved into three main components, peaking at 457(m), 503(main peak) and 556(sh) nm. The high-energy band, that appeared as only a trace for $Et_3PAu[SC_6H_4C(=O)NH_2\text{-}2]$ and $Ph_3PAu[SC_6H_4C(=O)NH_2\text{-}2]$ compounds under these conditions, gained intensity to become the major band for $Cy_3PAu[SC_6H_4C(=O)NH_2\text{-}2]$. The CIS post-HF calculations and the changes in the electron charges indicate that charge transfer from sulfur to the three p orbitals of gold are responsible for the observed luminescence. Furthermore, the splitting of the twofold p orbitals of gold by the vibronic interactions results in the appearance of three bands. In summary, from the foregoing it is apparent that the excitation and emission properties of organophosphinegold(I) thiolates are almost independent of the nature of the ancillary phosphines, regardless whether the phosphine is π-electron rich or not.

6. Sensitivity of luminescence to chemical media

Due to the variety in luminescence properties exhibited phosphinegold(I) compounds, including halides and thiolates, they have been utilized in exploring photochemical and photophysical processes in various media. A particularly notable application is the use of luminescent phosphinegold(I) thiolates as alkali metal ion sensors, an application that has been thoroughly reviewed previously [6,7]. In this section, the focus is directed towards the remarkable dependency of luminescence upon the pH of aqueous solution as well as upon solvent polarity.

As mentioned in Section 2, the three-coordinate $(TPA)_3AuCl$ compound is strongly luminescent in both the solid-state and in solution [30]. In aqueous solution, the luminescence of the compound is markedly enhanced with a quantum yield of 65% greater than that of the reference compound, namely $[Ru(2,2'\text{-bipyridyl})_3]^{2+}$. The intensity was reported to be very dependent on pH [66,67]. Thus, at pH < 3, the emission is totally absent. With increasing pH, the intensity increases but remains almost

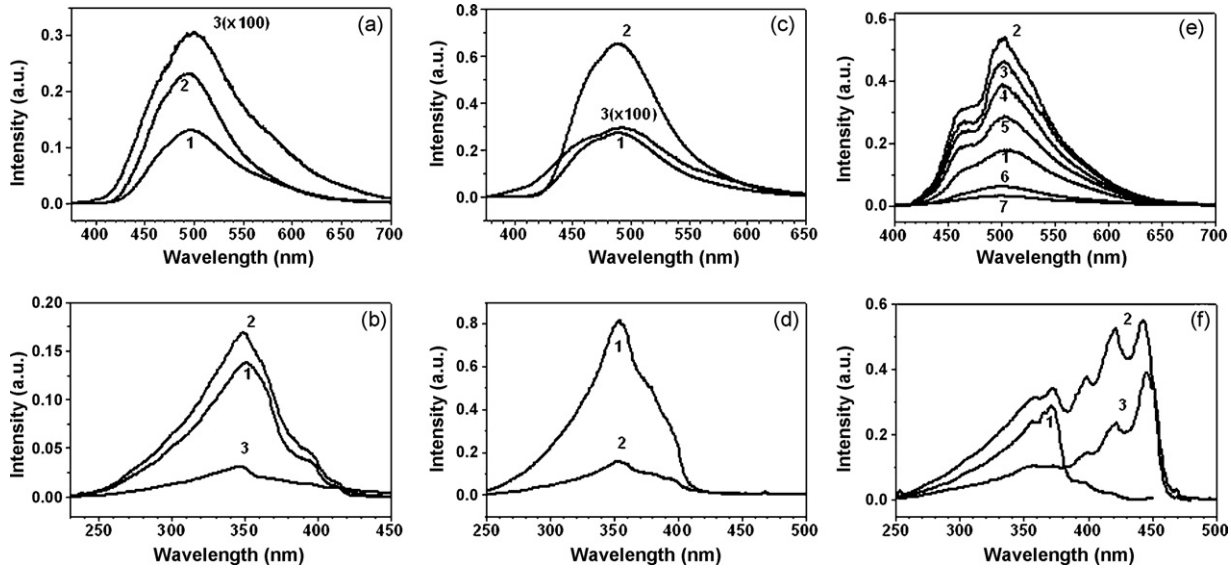

Fig. 27. (a) PL at $T = 10$ K (spectrum 1), 78 K (2) and RT (3), and (b) excitation at $T = 10$ K: $\lambda_{ems} = 497$ (spectrum 1) and 585 nm (2) spectra of $Et_3PAu[SC_6H_4C(=O)NH_2\text{-}2]$; (c) PL at $T = 10$ K (spectrum 1), 78 K (2) and RT (3), and (d) excitation at $T = 10$ K: $\lambda_{ems} = 490$ (spectrum 1) and 573 nm (2) spectra of $Ph_3PAu[SC_6H_4C(=O)NH_2\text{-}2]$; (e) PL at $T = 10$ K (spectrum 1), 50 K (2), 78 K (3), 100 K (4), 120 K (5), 140 K (6) and 160 K (7), and (f) excitation at $T = 10$ K: $\lambda_{ems} = 470$ (spectrum 1), 503 (2) and 574 nm (3) spectra of $Cy_3PAu[SC_6H_4C(=O)NH_2\text{-}2]$.Reprinted with permission from [65]. ©(2007) American Chemical Society.

unchanged in the pH range 6.5–10. The pH dependence of the luminescence intensity is likely due to protonation of the TPA ligand at one of the amine sites, resulting in the presence of various gold(I) species in aqueous solution.

The trinuclear compound of $[(8\text{-QNS})_2Au(AuPPh_3)_2]BF_4$ (8-QNS = quinoline-8-thiolate) further illustrates the strong solvent-dependence of the luminescence [68,69]. At room temperature in the solid-state, the complex salt produces a single emission band peaking at 587 nm. In solution, the cation produces one or two emission bands, as shown in Fig. 28. The origin of the high-energy band could be associated with Ph_3P and/or $AuPPh_3$ portions of the cation. Interestingly, it was shown that the low-energy band was quenched in polar solvents. The quenching rate increases in the order $CHCl_3 < THF < CH_3OH < CH_3CN$. This fascinating solvent-dependence of the low-energy emission was related to the presence of Au...Au interactions due to scrambling of the $[AuPPh_3]^+$ units (n.b. $[AuPPh_3]^+$ is isolobal to H^+) by assuming that the low-energy emission results from the S → Au charge transfer excited state modified by a gold-centered transition, see Scheme 1; crystallographic evidence was provided for the dinuclear cation and the trinuclear cation mediated by Au...Au interactions as illustrated in Fig. 29 [68,69].

The trinuclear compound $[Au(tppts)_3]^{8-}$, where tppts = tris-sulfonatophenyl phosphine, with a three coordinate trigonal planar geometry, also demonstrates similar luminescence properties in the solid-state and in aqueous solution, with room temperature emission maxima at 496 and 513 nm, respectively [67,70,71]. Fackler and co-workers found that the emission intensity of $[Au(tppts)_3]^{8-}$ in aqueous solution was very dependent on the dielectric constant. Thus, upon the addition of solvents with lower dielectric constants, the emission intensity is quenched. The authors suggested that this phenomenon could be due to the dissociation of the three coordinate species into a two coordinate species and three molar equivalents of the tppts anion (Eq. (1)):

$$[Au(tppts)_3]^{8-} \rightarrow [Au(tppts)_2]^{5-} + [tppts]^{3-} \quad (1)$$

This result gains in importance owing to the use of gold(I) thiolates and phosphinegold(I) thiolates in medicine, including their development as anti-tumor drugs [72]. It has been suggested that gold(I) species used in the treatment of rheumatoid arthritis quench singlet oxygen so that the removal of NO and O_2^- (a precursor of singlet option) prevents the buildup of toxic peroxynitrite (O_2NO^-) [70,71,73]. Continuing this theme, the $[Et_3PAu(TS)]$, where HTS = 5-(hydroxymethyl)-8-methyl-3-thiol-7-azacoumarin, compound was investigated. The molecular structure displays the expected feature (Fig. 30) and the crystal structure is stabilized primarily by O–H···O and O–H···S hydrogen bonding as well as weak aurophilic interactions [3.6056(9) Å]. The compound shows significantly better in vitro cytotoxicity than the widely used platinum(II) complex cisplatin, notably against the cisplatin-resistant cell line A2780cis. In the solid-state, this compound is weakly luminescent at room temperature and slightly more at 77 K [74]. In solution, the compound exhibits strong and complex luminescence behavior. Thus, in CH_2Cl_2 solution, $[Et_3PAu(TS)]$ yields one emission band, peaking at 440 nm, while in methanol solution, three bands appear at 425, 525 and 575 nm. The sensitivity of luminescence exhibited by gold compounds to chemical environments and the chemical reactivity of the gold(I) compounds, including drug action

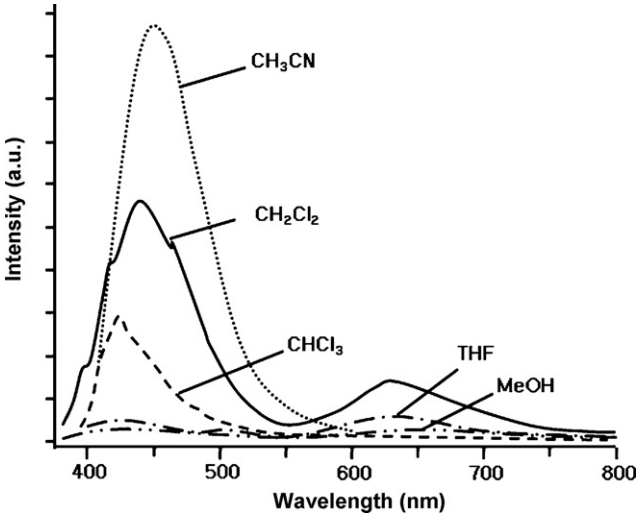

Fig. 28. Emission spectra of $[(8\text{-QNS})_2Au(AuPPh_3)_2]BF_4$ measured in various solvents (CH_3CN, CH_2Cl_2, $CHCl_3$, THF, and MeOH) at 298 K. Concentration = 9×10^{-5} M. Excitation is at 320 nm. Reprinted with permission from [69]. ©(2003) American Chemical Society.

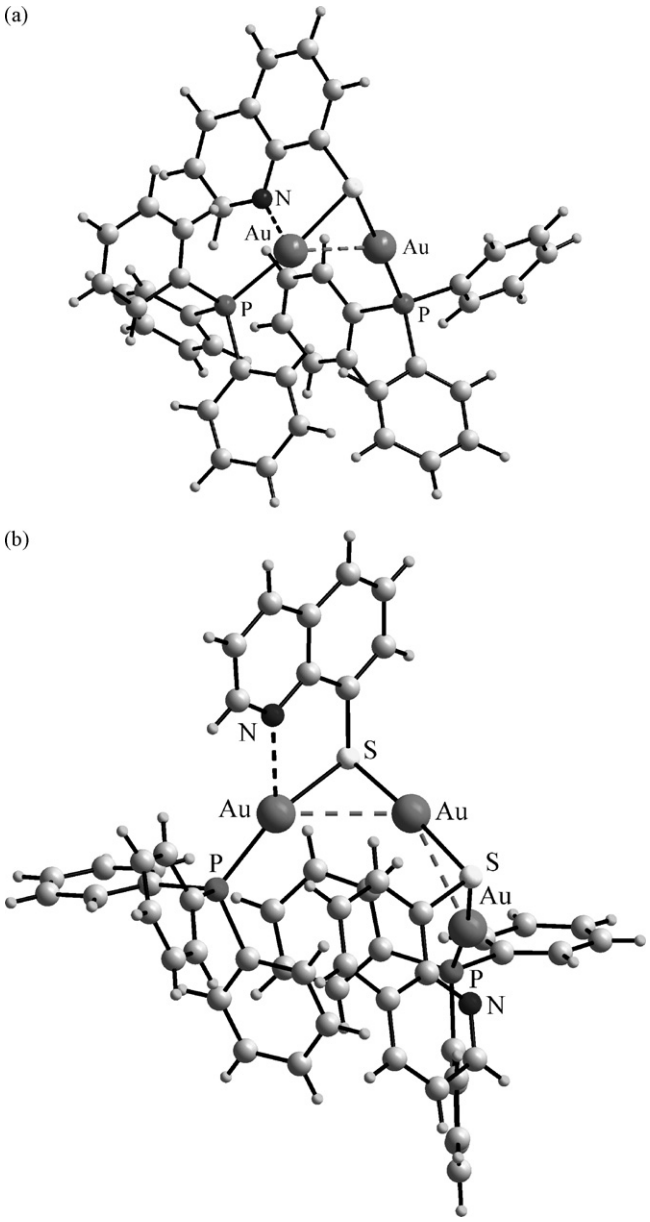

Fig. 29. Molecular structures of the monocationic species: (a) $[(8\text{-QNS})(AuPPh_3)_2]$ [68]; and (b) dinuclear $[(8\text{-QNS})_2Au(AuPPh_3)_2]$ [69]; aurophilic interactions are represented by dashed lines.

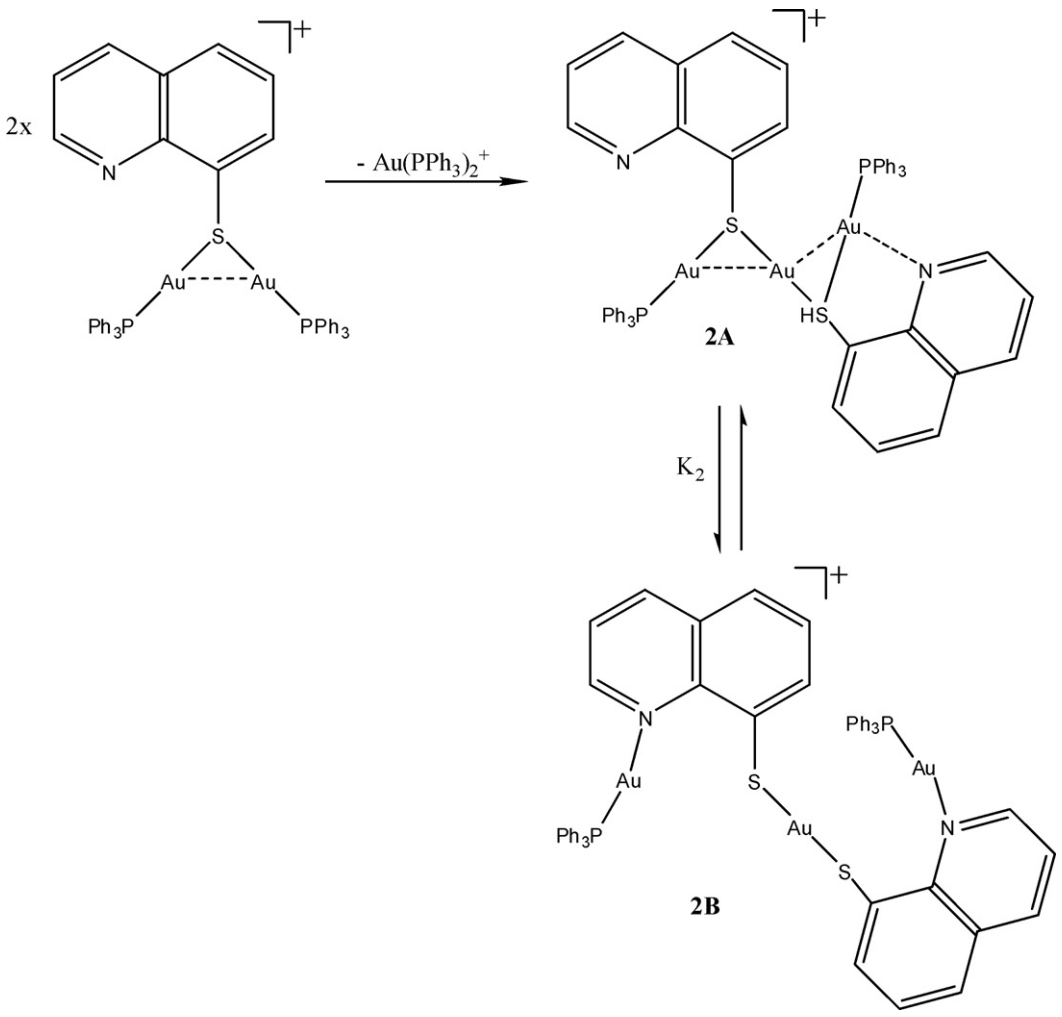

Scheme 1.

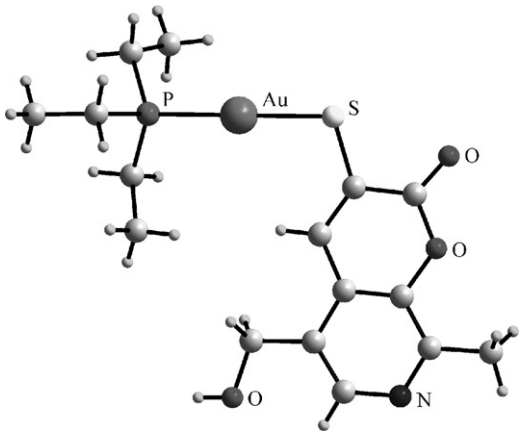

Fig. 30. Molecular structure of [$Et_3PAu(TS)$] [74].

and photochemical reactions, have long been assumed to be associated with the characters of the HOMO and LUMO electronic states [70,75–78].

7. Concluding remarks

In this review, the focus has been upon the luminescence properties of various phosphinegold(I) halides and thiolates, a significant sub-class of gold(I) compounds. The demonstrated variety in their luminescence properties can be understood by a careful examination of their structural properties allied to quantum mechanical calculations on their electronic structures. There is still an enormous scope for continued investigation and development of the luminescence properties of gold(I) compounds, in particular on high-nuclearity clusters, especially considering the potential of these compounds to function as environmental sensors and therapeutic agents, the aesthetic beauty of their structures notwithstanding as a motivating factor.

Acknowledgments

J.-G.K. thanks Kumho Electric Inc. for a financial support and acknowledges the fellowships of the BK 21 program.

References

[1] J.M. Forward, J.P. Fackler Jr., Z. Assefa, in: D.M. Roundhill, J.P. Fackler Jr. (Eds.), Optoelectronic Properties of Inorganic Compounds, Plenum Press, New York, 1999 (Chapter 6, pp. 195–229).
[2] E.Y. Fung, M.M. Olmstead, J.C. Vickery, A.L. Balch, Coord. Chem. Rev. 171 (1998) 151.
[3] V.W.-W. Yam, C.-L. Chan, C.-K. Li, K.M.-C. Eong, Coord. Chem. Rev. 216–217 (2001) 173.
[4] R.C. Evans, P. Douglas, C.J. Winscom, Coord. Chem. Rev. 250 (2006) 2093.
[5] Y.-A. Lee, R. Eisenberg, J. Am. Chem. Soc. 125 (2003) 7778.
[6] V.W.-W. Yam, E.C.-C. Cheng, Top. Curr. Chem. 281 (2007) 269.
[7] V.W.-W. Yam, E.C.-C. Cheng, Chem. Soc. Rev. 37 (2008) 1806.

[8] H. Schmidbaur, Chem. Soc. Rev. 24 (1995) 391.
[9] M.J. Katz, D.B. Leznoff, Chem. Soc. Rev. 37 (2008) 1884.
[10] P. Pyykkö, Angew. Chem. Int. Edn. 43 (2004) 4412.
[11] H. Schmidbaur, S. Cronje, B. Djordjevic, O. Schuster, Chem. Phys. 311 (2005) 151.
[12] H. Schmidbaur, Nature (London) 413 (2001) 31.
[13] W.E. van Zyl, J.M. Lopez-de-Luzuriaga, J.P. Fackler Jr., J. Mol. Struct. 516 (2000) 99.
[14] J.A. Muir, M.M. Muir, L.B. Pulgar, P.G. Jones, G.M. Sheldrick, Acta Crystallogr. C41 (1985) 1174.
[15] E.R.T. Tiekink, Acta Crystallogr. C45 (1989) 1233.
[16] F.S. Kuan, S.Y. Ho, P.P. Tadbuppa, E.R.T. Tiekink, CrystEngComm 10 (2008) 548.
[17] N.C. Baenziger, W.E. Bennett, D.M. Soboroff, Acta Crystallogr. C32 (1976) 962.
[18] (a) P.F. Barron, L.M. Engelhardt, P.C. Healy, J. Oddy, A.H. White, Aust. J. Chem. 40 (1987) 1545;
(b) L.G. Kuz'mina, N.V. Dvortsova, Zh. Neorg. Khim. (Russ. J. Inorg. Chem.) 36 (1991) 2021.
[19] S. Ahrland, K. Dreisch, B. Noren, A. Oskarsson, Acta Chem. Scand. A41 (1987) 173.
[20] (a) C.S.W. Harker, E.R.T. Tiekink, Acta Crystallogr. C46 (1990) 1546;
(b) R.C. Bott, P.C. Healy, G. Smith, Aust. J. Chem. 57 (2004) 213.
[21] L.J. Larson, E.M. McCauley, B. Weissbart, D.S. Tinti, J. Phys. Chem. 99 (1995) 7218.
[22] J.-G. Kang, C. Park, E.R.T. Tiekink, Bull. Kor. Chem. Soc. 27 (2006) 299.
[23] (a) M.A. Buntine, V.J. Hall, F.J. Kosovel, E.R.T. Tiekink, J. Phys. Chem. A 102 (1998) 2472;
(b) E.R.T. Tiekink, V.J. Hall, M.A. Buntine, J. Hook, Z. Kristallogr. 215 (2000) 23;
(c) M.I. Mohamed-Ibrahim, S. See Chee, M.A. Buntine, M.J. Cox, E.R.T. Tiekink, Organometallics 19 (2000) 5410;
(d) M.A. Buntine, F.J. Kosovel, E.R.T. Tiekink, CrystEngComm 5 (2003) 331.
[24] (a) J. Li, P. Pyykkö, Chem. Phys. Lett. 197 (1992) 586;
(b) P. Pyykkö, P. Zaleski-Ejgierd, J. Chem. Phys. 128 (2008) 124309.
[25] P.D. Cookson, E.R.T. Tiekink, Acta Crystallogr. C49 (1993) 1602.
[26] D.V. Toronto, B. Weissbart, D.S. Tinti, A.L. Balch, Inorg. Chem. 35 (1996) 2484.
[27] B. Weissbart, D.V. Toronto, A.L. Balch, D.S. Tinti, Inorg. Chem. 35 (1996) 2490.
[28] C. King, J.-C. Wang, N.I. Md. Khan, J.P. Fackler Jr., Inorg. Chem. 28 (1989) 2145.
[29] Z. Assefa, M.A. Omary, B.G. McBurnett, A.A. Mohamed, H.H. Patterson, R.J. Staples, J.P. Fackler Jr., Inorg. Chem. 41 (2002) 6274.
[30] Z. Assefa, B.G. McBurnett, R.J. Staples, J.P. Fackler Jr., B. Assmann, K. Angermaier, H. Schmidbaur, Inorg. Chem. 34 (1995) 75.
[31] Z. Assefa, B.G. McBurnett, R.J. Staples, J.P. Fackler Jr., Inorg. Chem. 34 (1995) 4965.
[32] W.-F. Fu, K.-C. Chan, V.M. Miskowski, C.-M. Che, Angew. Chem. Int. Ed. 38 (1999) 2783.
[33] W.-F. Fu, K.-C. Chan, K.-K. Cheung, C.-M. Che, Chem. Eur. J. (2001) 4656.
[34] H.-R.C. Jaw, M.M. Savas, R.D. Rogers, W.R. Mason, Inorg. Chem. 28 (1989) 1028.
[35] M.A. Bennett, S.K. Bhargava, D.C.R. Hockless, L.L. Welling, A.C. Willis, J. Am. Chem. Soc. 118 (1996) 10469.
[36] H. Xiao, Y.-X. Weng, W.-T. Wong, T.C.W. Mak, C.-M. Che, J. Chem. Soc., Dalton Trans. (1997) 221.
[37] H.-X. Zhang, C.-M. Che, Chem. Eur. J. 7 (2001) 4887.
[38] A. Stutzer, P. Bissinger, H. Schmidbaur, Chem. Ber. 125 (1992) 367.
[39] T. Tanase, K. Masuda, J. Matsuo, M. Hamaguchi, R. Ara Begum, S. Yano, Inorg. Chim. Acta 299 (2000) 91.
[40] B.-Ch. Tzeng, J. Zank, A. Schier, H. Schmidbaur, Z. Naturforsch. B54 (1999) 825.
[41] M. Bardaji, A. Laguna, J. Vicente, P.G. Jones, Inorg. Chem. 40 (2001) 2675.
[42] A.L. Balch, E.Y. Fung, Inorg. Chem. 29 (1990) 4764.
[43] D. Fernández, M.I. García-Seijo, M. Bardají, A. Laguna, M.E. García-Fernández, Dalton Trans. (2008) 2633.
[44] G.A. Bowmaker, J.C. Dyason, P.C. Healy, L.M. Engelhardt, C. Pakawatchai, A.H. White, J. Chem. Soc. Dalton Trans. (1974) 1089.
[45] N.C. Baenziger, K.M. Dittemore, J.R. Doyle, Inorg. Chem. 13 (1974) 805.
[46] M. Hoshino, H. Uekusa, Y. Ohashi, Bull. Chem. Soc. Jpn. 79 (2006) 1362.
[47] S. Rudolph, I.-P. Lorenz, K. Polborn, Private Communication to the Cambridge Crystallographic Data Centre (2005).
[48] R.J. Staples, C. King, M.N.I. Khan, R.E.P. Winpenny, J.P. Fackler Jr., Acta Crystallogr. C49 (1993) 472.
[49] P.G. Jones, Acta Crystallogr. C36 (1980) 3105.
[50] P. Sinha, A.K. Wilson, M.A. Omary, J. Am. Chem. Soc. 127 (2005) 12488.
[51] C. King, M.N.I. Khan, R.J. Staples, J.P. Fackler Jr., Inorg. Chem. 31 (1992) 3236.
[52] K.A. Barakat, T.R. Cundari, M.A. Omary, J. Am. Chem. Soc. 125 (2003) 14228.
[53] O. Crespo, M.C. Gimeno, P.G. Jones, A. Laguna, Inorg. Chem. 35 (1996) 1361.
[54] M.J. Calhorda, O. Crespo, M.C. Gimeno, P.G. Jones, A. Laguna, J.M. López-de-Luzuriaga, J.L. Perez, M.A. Ramón, L.F. Veiros, Inorg. Chem. 39 (2000) 4280.
[55] O. Crespo, M.C. Gimeno, P.G. Jones, A. Laguna, J.M. López-de-Luzuriaga, M. Monge, J.L. Pérez, M.A. Ramón, Inorg. Chem. 42 (2003) 2061.
[56] D. Zhang, J. Dou, D. Li, Dacheng, D. Wang, J. Coord. Chem. 60 (2007) 825.
[57] F.A. Cotton, G. Murillo, M. Bochmann, Advanced Inorganic Chemistry, 6th edition, Wiley, New York, 1999, p. 643.
[58] R. Narayanaswamy, M.A. Young, E. Parkhurst, M. Ouellette, M.E. Kerr, D.M. Ho, R.C. Elder, A.E. Bruce, M.R.M. Bruce, Inorg. Chem. 32 (1993) 2506.
[59] W.B. Jones, B.J. Yuan, R. Narayanaswamy, M.A. Young, R.C. Elder, A.E. Bruce, M.R.M. Bruce, Inorg. Chem. 34 (1995) 1996.
[60] M. Forward, D. Bohmann, J.P. Fackler Jr., R.J. Staples, Inorg. Chem. 34 (1995) 6330.
[61] J.P. Fackler Jr., R.J. Staples, A. Elduque, T. Grant, Acta Crystallogr. C50 (1994)520.
[62] S.Y. Ho, E.C.-C. Cheng, E.R.T. Tiekink, V.W.-W. Yam, Inorg. Chem. 45 (2006)8165.
[63] B.-C. Tzeng, Y.-C. Huang, W.-M. Wu, S.-Y. Lee, G.-H. Lee, S.-M. Peng, Cryst. Growth Des. 4 (2004) 63.
[64] S.-S. Yun, J.-K. Kim, J.-S. Jung, C. Park, J.-G. Kang, D.R. Smyth, E.R.T. Tiekink, Cryst. Growth Des. 6 (2006) 899.
[65] J.-G. Kang, H.-K. Cho, C. Park, S.-S. Yun, J.-K. Kim, G.A. Broker, D.R. Smyth, E.R.T. Tiekink, Inorg. Chem. 46 (2007) 8228.
[66] J.M. Forward, Z. Assefa, J.P. Fackler Jr., J. Am. Chem. Soc. 117 (1995) 9103.
[67] Z. Assefa, J.M. Forward, T.A. Grant, R.J. Staples, B.E. Hanson, A.A. Mohamed, J.P. Fackler Jr., Inorg. Chim. Acta 352 (2003) 31.
[68] B.-C. Tzeng, C.-K. Chan, K.-K. Cheung, C.-M. Che, S.-M. Peng, Chem. Commun. (1997) 135.
[69] B.-C. Tzeng, H.-T. Yeh, Y.-C. Huang, H.-Y. Chao, G.-H. Lee, S.-M. Peng, Inorg. Chem. 42 (2003) 6008.
[70] J.P. Fackler Jr., T.A. Grant, B.E. Hanson, R.J. Staples, Gold Bull. (London) 32 (1999) 20.
[71] J.P. Fackler Jr., Z. Assefa, J.M. Forward, T.A. Grant, Metal-Based Drugs 6 (1999) 223.
[72] (a) E.R.T. Tiekink, Crit. Rev. Oncol./Hematol. 42 (2002) 225;
(b) E.R.T. Tiekink, Gold Bull. 36 (2003) 117;
(c) E.R.T. Tiekink, Inflammopharmacology 16 (2008) 138.
[73] E.J. Corey, M.M. Mahrotra, A.U. Khan, Science 236 (1987) 68.
[74] J.S. Casas, E.E. Castellano, M.D. Couce, O. Crespo, J. Ellena, A. Laguna, A. Sánchez, J. Sordo, C. Taboada, Inorg. Chem. 46 (2007) 6236.
[75] Y. Ma, X. Zhou, J. Shen, H.-Y. Chao, C.-M. Che, Appl. Phys. Lett. 74 (1999) 1361.
[76] T. Jiang, G. Wei, C. Turmel, A.E. Bruce, M.R.M. Bruce, Metal-Based Drugs 1 (1994) 419.
[77] J.B. Foley, A.E. Bruce, M.R.M. Bruce, J. Am. Chem. Soc. 117 (1995) 9596.
[78] J.B. Foley, S.E. Gay, M.J. Vela, B.M. Foxman, A.E. Bruce, M.R.M. Bruce, Eur. J. Inorg. Chem. (2007) 4946.